

UNIVERSITY OF NAPOLI FEDERICO II
Dipartimento di Biologia e Patologia Cellulare e
Molecolare “L. Califano”

Doctorate School in Molecular Medicine

Doctorate Program in
Genetics and Molecular Medicine
Coordinator: Prof. Lucio Nitsch
Tutor: Prof. Francesco Salvatore
Co-tutor: Prof.ssa Giulia Frisso
XXIII Cycle

Molecular Basis of Cardiac Arrhythmias:
Genetics of Natural Variants and
Electrophysiological Investigation
of Mutant Proteins

Dott. Nicola Detta



Napoli 2010

UNIVERSITY OF NAPOLI FEDERICO II

Doctorate School in Molecular Medicine

**Doctorate Program in
Genetics and Molecular Medicine
XXIII Cycle**

Thesis carried out at

**CEINGE-Biotecnologie Avanzate
and
Dipartimento di Biochimica e Biotecnologie Mediche**

**Molecular Basis of Cardiac Arrhythmias:
Genetics of Natural Variants and
Electrophysiological Investigation
of Mutant Proteins**



Napoli 2010

*To my parents
who supported my scientific inquiry*

**Molecular Basis of Cardiac Arrhythmias:
Genetics of Natural Variants and
Electrophysiological Investigation
of Mutant Proteins**

TABLE OF CONTENTS

ABSTRACT	Page	4
CHAPTER 1 – BACKGROUND		5
1.1 Inherited arrhythmogenic disorders		5
1.2 Cardiac electrophysiology		5
1.3 Long QT syndrome		10
1.4 Brugada syndrome		13
1.5 Protein related to long QT syndrome and Brugada Syndrome		15
1.5.1 Cardiac sodium channel		15
1.5.2 Potassium channels		17
1.5.2.1 HERG: rapid rectifier delayed potassium channel		18
1.5.2.2 KCNQ1: slow rectifier delayed potassium channel		19
1.5.3 Beta subunit of potassium channels: MiRP and MinK		21
CHAPTER 2 – TECHNICAL BACKGROUND		22
2.1 Why the patch clamp?		22
2.1.1 Basic information		22
2.1.2 The patch clamp technique		23
2.1.3 Whole-cell patch clamp		25
2.1.4 Fabrication of patch pipettes		27
2.1.5 Patch clamp protocols		27
CHAPTER 3 - AIM OF THE STUDY		29
CHAPTER 4 - MATERIALS AND METHODS		30
4.1 Patients and control population		30
4.2 Genomic DNA extraction and PCR		30
4.3 Mutation screening: dHPLC and DNA sequencing		34
4.4 RNA extraction		34
4.5 Reverse transcriptase-PCR		34
4.6 Minigene: construction and expression		36
4.7 Site-directed mutagenesis		37
4.8 Cell cultures and heterologous expression		39
4.9 Immunofluorescence		39
4.10 Electrophysiology		40
4.11 Data analysis		41
CHAPTER 5 – RESULTS		42
5.1 Genetic analysis		42
5.2 Splicing analysis in one patient carrying the mutation SCN5A c.G3964T		45
5.3 Immunofluorescence studies		46
5.4 Functional characterization of mutant channels		48
5.4.1 Biophysical properties of mutant hH1-N1472del		48

5.4.2 Electrophysiological analysis of digenic heterozygosity in KCNQ1 and KCNH2 genes	53
5.4.2.1 Biophysical properties of mutant HERG-p.C108Y	53
5.4.2.2 Biophysical properties of mutant KCNQ1-p.R583H	56
CHAPTER 6 - DISCUSSION	60
6.1 Gain-of-function of mutant hH1-p.ΔN1472	60
6.2 Digenic heterozygosity in KCNH2 and KCNQ1 genes	61
ABBREVIATIONS	63
ACKNOWLEDGEMENTS	66
REFERENCES	67

ABSTRACT

Channelopathies are diseases caused by deranged functioning of ion channel subunits or the proteins that regulate them. Long QT and Brugada syndrome are included in this group. In particular, long QT syndrome (LQTS) is a familial autosomal dominant disease characterized by prolongation of the QT interval on the surface ECG, syncope, torsade de pointes and sudden cardiac death in young patients. Each type of heritable LQTS (LQTS 1-12) is linked to mutations in a specific gene. Mutations occur more frequently in the cardiac ion channel coding genes (SCN5A, KCNH2, KCNQ1) and ancillary β -subunits (KCNE1 and KCNE2). Differently, BrS is an inherited cardiac disease characterized by ST segment elevation in the right precordial leads (V1 to V3), susceptibility to ventricular tachyarrhythmia and sudden cardiac death, typically during rest or sleep. BrS is inherited as an autosomal dominant trait and its prevalence in Caucasians is 5/1000. The disorder is linked to mutations in the SCN5A gene. Our project was designed to functionally characterize the novel mutations found in genes related to LQTS and BrS to better understand the pathogenesis of pathological phenotypes.

To this aim, we first amplified by PCR all coding exons, 5' and 3' UTR of the SCN5A, KCNQ1, KCNH2, KCNE1 and KCNE2 genes and analyzed them by dHPLC and automatic sequencing. The mutants were generated by QuickChange site-directed mutagenesis. Mutants were transiently transfected in mammalian cells for in vitro analysis.

We characterized the LQT3 associated p. Δ N1472 mutation that we found in SCN5A gene. The electrophysiological studies demonstrated that the hH1 mutation had a shift in the voltage-dependence of inactivation, a positive shift in the voltage dependence of activation and a slower recovery from inactivation compared to WT channel. Moreover, the persistent current levels were much higher in SCN5A-p. Δ N1472 than in the WT channel.

We also studied mutations KCNH2-p.C108Y and KCNQ1-p.R583H. Interestingly, only subjects carrying both mutations manifested severe LQTS. The biophysical studies showed that in the homozygous condition, KCNH2-p.C108Y, led to a non-functional KCNH2 channel, whereas, in the heterozygous condition, mutant KCNH2 had a significantly reduced current density and a negative shift in the voltage dependence of activation compared to the WT. Furthermore, mutant KCNQ1-p.R583H had a significantly reduced tail current density compared to the WT channel, but no significant changes in activating current density and in voltage-dependence of activation. In conclusion, we demonstrate that the SCN5A-p. Δ N1472 and KCNH2-p.C108Y mutants exhibit characteristic biophysical properties causing LQTS; whereas KCNQ1-p.R583H, in combination with KCNE1-WT, does not exhibit striking biophysical defects, but in combination with mutant KCNH2 it results in a more severe phenotype. Our results allow to better understand the pathogenesis of LQTS phenotype and to increase the knowledge of ion channel behavior in the pathological conditions.

Chapter 1

BACKGROUND

1.1 Inherited Arrhythmogenic Disorders

The term “inherited arrhythmogenic disorders” identifies a group of genetically determined diseases characterized by the presence of a vulnerable substrate that may lead to the onset of malignant ventricular tachyarrhythmia and sudden death in a structurally normal heart [Priori et al. 2003]. The arrhythmogenic disorders are the major cause of mortality and morbidity in developed nations. Inherited cardiac arrhythmias generally result from abnormalities in four classes of proteins [Antzelevitch 2003]:

1. Ion channel protein abnormalities, which cause arrhythmias due to a defect in transport of ions, like sodium and potassium across the cell membrane;
2. Abnormalities in cell-to-cell junctional proteins causing arrhythmogenic right ventricular cardiomyopathy/dysplasia (ARVC/D); (the complete list of abbreviations is on pages 63-65);
3. Contractile sarcomere protein abnormalities causing hypertrophic cardiomyopathy (HCM);
4. Cytoskeletal proteins abnormalities triggering Familial Dilated Cardiomyopathy (FDCM) [Vohra 2007].

Most, but not all of these disorders are caused by mutations in genes encoding cardiac ion channel proteins [Wolf and Berul 2008].

In recent years, the discovery of pathogenic mutations in inherited arrhythmia syndromes has provided novel insights for the understanding and treatment of diseases predisposing to sudden cardiac death (SCD). Among family members carrying an identical mutation in a single gene, remarkable phenotypic variability and expressivity may be observed, suggesting both environmental and genetic modifiers [Priori 2004, Brink et al. 2005].

1.2 Cardiac Electrophysiology

In order to ensure appropriate coupling between cardiac excitation and the subsequent contraction of the myocardium, initiation and propagation of the electrical stimulation have to be accurately timed and have to follow a specific pathway. The normal cardiac electrical activity starts by the spontaneous excitation of “pacemaker” cells in the sinoatrial node (SAN) in the right

atrium. By traveling through intercellular gap junctions, the excitation wave depolarizes adjacent atrial myocytes, ultimately resulting in excitation of the atria. Next, the excitation wave propagates via the atrioventricular node (AVN) and the Purkinje fibers to the ventricles, where ventricular myocytes are depolarized, resulting in excitation of the ventricles. On the surface electrocardiogram, atrial and ventricular excitation are represented by the P wave and the QRS complex (fig. 1 A and B), respectively, depolarization of each atrial or ventricular myocyte is represented by the initial action potential upstroke, where the negative resting membrane potential (approximately -85mV) depolarizes to positive voltages. Afterwards, restitution of the resting membrane potential results in atrial and ventricular repolarization [Amin et al. 2010].

The normal electrophysiologic behavior of the heart is determined by ordered propagation of excitatory stimuli resulting in rapid depolarization and slow repolarization, generating action potentials in individual myocytes [Roden et al. 2002]. These action potentials initiate and coordinate contraction, making possible the function of the heart as a pump [Fozzard and Haber 1991]. The cardiac action potential consists in 5 phases (fig. 1 C):

- ✓ Phase 0 is the phase of rapid depolarization. The membrane potential shifts into positive voltage range. This phase is central to rapid propagation of the cardiac impulse. This phase is initiated by the rapid opening (activation) of voltage-gated sodium channels.

- ✓ Phase 1 is a phase of rapid repolarization. This phase sets the potential for the next phase of the action potential. Phase 1 of the cardiac action potential occurs immediately after the peak of depolarization and is recognized as a partial repolarization of the membrane. This small repolarizing effect is due to the closure (inactivation) of cardiac sodium channels, and activation of transient outward potassium current (I_{kto}).

- ✓ Phase 2, a plateau phase, is the longest phase. The relative long duration of this phase is unique to ventricular and Purkinje fiber myocytes. The plateau is generated primarily by slowly decreasing inward calcium currents through L-type calcium channels and gradually increasing outward current through several types of potassium channels. The total amount of current during the plateau phase of the cardiac action potential is small. As a consequence, relatively small changes in ion current during this phase can have a major impact on action potential duration. At this point in the cardiac cycle the ECG has returned to baseline

- ✓ Phase 3 is the phase of rapid repolarization that restores the membrane potential to its resting value. This effect is mediated by outward potassium currents. There are two main repolarizing potassium currents, I_{Kr} and I_{Ks} that sum to terminate the plateau phase and initiate final repolarization. I_{Kr} and I_{Ks} are the rapidly and slowly activating delayed rectifier potassium current respectively. The repolarization phase correlates with T-wave on surface ECG.

✓ Phase 4, or the resting potential, is the final phase of action potential and is stable at ≈ -90 mV in normal working myocardial cells. This phase represents ventricular relaxation or diastole and is indicated on the ECG as a return to baseline [Keating and Sanguinetti 2001].

The membrane potential at the onset of phase 4 is more depolarized (-50 to -65 mV), undergoes slow diastolic depolarization, and gradually merges into phase 0 [Grant 2009].

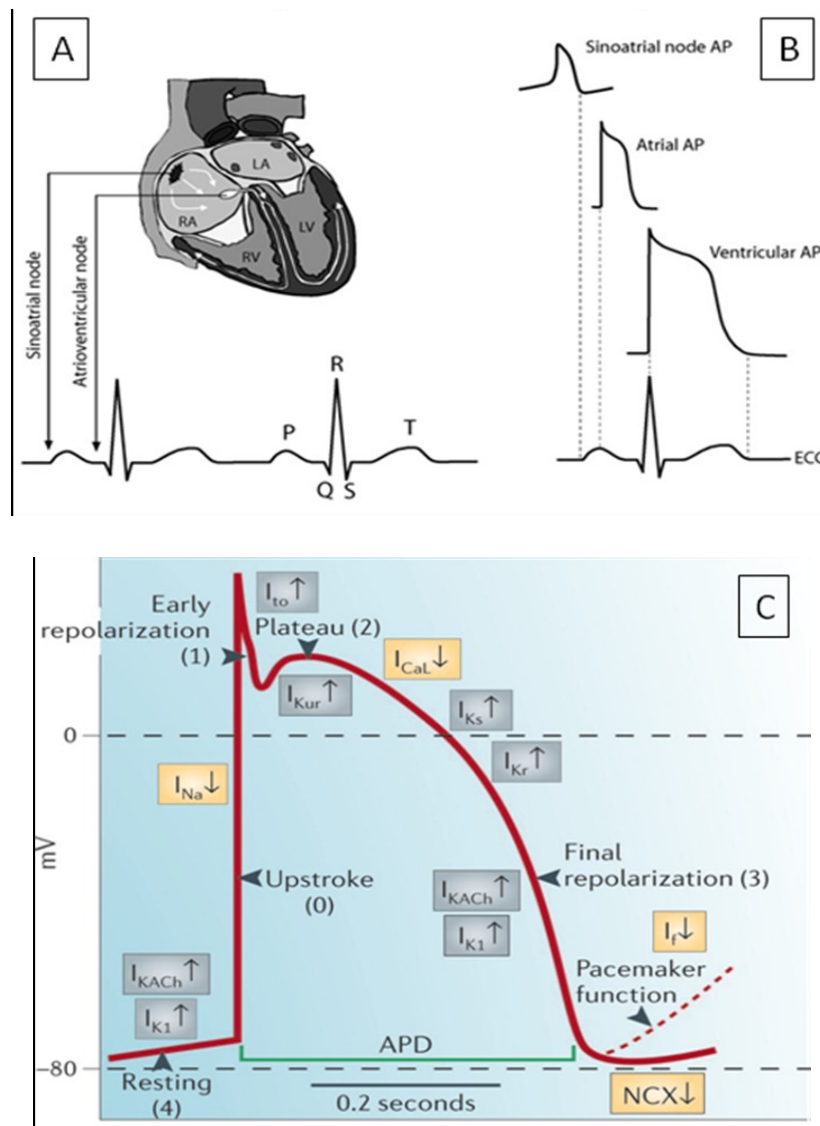


Figure 1: Cardiac electrical activities. A, Schematic representation of the electrical conduction system correlated with electrocardiogram (ECG). B, Relationship between ECG and action potential (AP) of myocytes from different cardiac regions. C, Schematic representation of cardiac action potential phases. (APD = action potential duration).

Action potential configuration and durations vary in specific regions (e.g., atrium versus ventricle) as well as in specific areas within those regions. Epicardial cells in the ventricle demonstrate a prominent phase 1 notch, which is much less prominent in the endocardium [Antzelevitch 2000]. Purkinje and midmyocardial cells display a phase 1 notch and action potentials that are much longer than those in epicardium. Such physiologic heterogeneities likely reflect variations in expression or function of the repertoire of ion channels and other proteins that constitute cardiac ion currents [Roden et al. 2002]. Therefore, defects in ion channel currents can distort the action potential creating the substrate for the development of cardiac arrhythmias.

The cardiac ion channels are proteins and glycoproteins forming transmembrane pores that permit the flow of ions along the electrochemical gradient that exists across the plasma membrane [Antzelevitch 2003]. These proteins generally consist in a primary pore forming α -subunit and an accessory β -subunit.

The cardiac ion channels have two fundamental properties:

1. Ion permeation, and
2. Gating [Langer 1997].

1. Ion permeation describes the movement through the open channel; in particular, the selective permeability of ion channels to specific ions is a basis of classification of ion channels (e.g. Na^+ , K^+ channels). Ion channels do not function as simple fluid-filled pores, but provide multiple binding sites for ions as they traverse the membrane. Ions become dehydrated as they cross the membrane, as ion-binding site interaction is favored over ion-water interaction.

The equivalent circuit model of an ion channel is that of a resistor. Simple resistors have a linear relationship between ΔV and current I that is $I = \Delta V / R = \Delta V g$ (Ohm's Law); where I is the current magnitude, ΔV is the electrochemical potential, R is the electrical resistance, and g is the conductance that measures how easily electricity flows along a certain path through an electrical element. Actually, most ion channels have a nonlinear current-voltage relationship, indeed, for the same absolute value of ΔV , the magnitude of the current depends on the direction of ion movement into or out of the cells.

2. Gating is the mechanism of opening and closing of ion channels. Ion channels are sub-classified by their mechanism of gating: voltage-dependent, ligand-dependent and mechano-sensitive gating.

Voltage-dependent gating is the commonest mechanism of gating observed in ion channels. Voltage-gated ion channels change their conductance in response to variations in membrane potential; a majority of ion channels opens in response to membrane depolarization.

Ligand-dependent gating is the second major gating mechanism of cardiac ion channels. These channels open or close depending on binding of ligands to the channel. The mechano-sensitive (or stretch-activated) channels can

transduce a physical input, such as stretch, into an electric signal through a change in channel conductance [Grant 2009].

A channel may have three several different states (corresponding to different conformations of the protein):

- Close state, during rest potential;
- Open state, triggered by membrane depolarization; and
- Inactivated state.

Inactivation is a non-conducting state of channels during depolarization. Two major types of inactivation are described: N-type inactivation (known as “ball and chain”) that is dependent on intracellular N-terminal inactivation gate that obstruct the inner pore, and C-type inactivation involving a rearrangement of residues in or near the pore; apparently this type of inactivation closes a gate at the “extracellular” end of the pore (fig. 2). Thus, despite its name, C-type inactivation is not especially dependent on the C-terminus of the channel. The N-type inactivation is responsible of fast inactivation, whereas C-type is linked to slow inactivation [Roden et al. 2002; Hille 2001]. The inactivation is the basis for refractoriness in cardiac muscle and is fundamental for the prevention of premature re-excitation. To regain the ability to open, the channel must undergo a recovery process at hyperpolarized potentials [Roden et al. 2002].

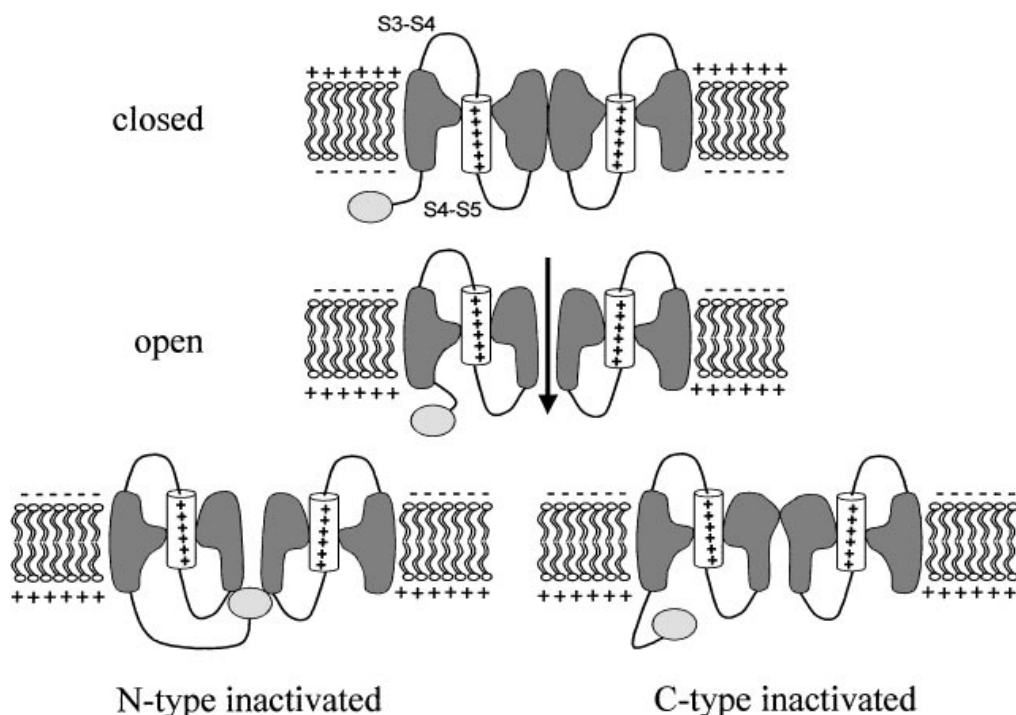


Figure 2: Transition state of voltage-gated ion channel reflecting changes in the conformation of the channel protein complex.

At cellular level, the formation of the heartbeat, as well as cardiac force development, are both directly regulated by the cardiac action potential, which depends on the coordinated actions of a large number of distinct sarcolemmal ion channels [Antzelevitch 2000]. The generation of action potential is the result of the selective permeability of the ion channels distributed on the cell membrane. During the action potential, the permeability of ion channels changes and each ion moves passively down its electro-chemical gradient ($\Delta V = [V_m - V_{ion}]$, where ΔV is the electrochemical potential, V_m is the membrane potential and V_{ion} is the reversal potential of a specific ion) to change the membrane potential of the cell. The membrane potential is established by an unequal distribution of electrically charged ions across the sarcolemmal and the presence of conducting ion channels on the cell membrane [Amin et al. 2010; Grant 2009]. Alterations in the function of ion channels, either a gain or loss in function, due to genetic mutation can result in cardiac arrhythmia. For example, a gain in function of the sodium channel due to mutation in sodium channel gene causes Long QT syndrome type 3 whereas a decrease in function in the same channel can cause Brugada syndrome [Vohra 2007].

1.3 Long QT Syndrome

Long QT syndrome (LQTS) is a cardiac channelopathy characterized by prolonged QT intervals on the surface electrocardiogram (ECG) (fig. 3), syncope and sudden cardiac death due to ventricular tachyarrhythmias, in particular torsade de pointes [Amin et al. 2009, Schwartz et al. 2001]. The disorder occurs in structurally normal heart and usually manifests in children and teen-agers. This genetic channelopathy has variable penetrance. The estimated overt prevalence of this disorder is in the range of about 1:5000 subjects. Prolonged QT intervals reflect action potential duration in ventricular myocytes, and correspond with delayed ventricular repolarization [Amin et al. 2009]. Cardiac events are often precipitated by physical or emotional stress even if in a smaller subset of individuals cardiac events occur at rest. For this reason, antiadrenergic intervention with beta-blockers is the cornerstone of therapy in the LQTS [Goldenberg et al. 2008]. The pathological QTc values for men and women must be more than 440 and 460 milliseconds, respectively [Schwartz et al. 1993]. Heritable LQTS is classified into 12 different types and each type is linked to mutations in a gene encoding a protein that is directly (ion channel) or indirectly (β -subunit or regulatory protein) involved in repolarization [Morita et al. 2008].

The syndrome is transmitted most often in families as an autosomal dominant trait (Romano-Ward syndrome) and less commonly as an autosomal recessive disease combined with congenital sensorineural deafness (Jervell and Lange-Nielsen syndrome) [George 2005].

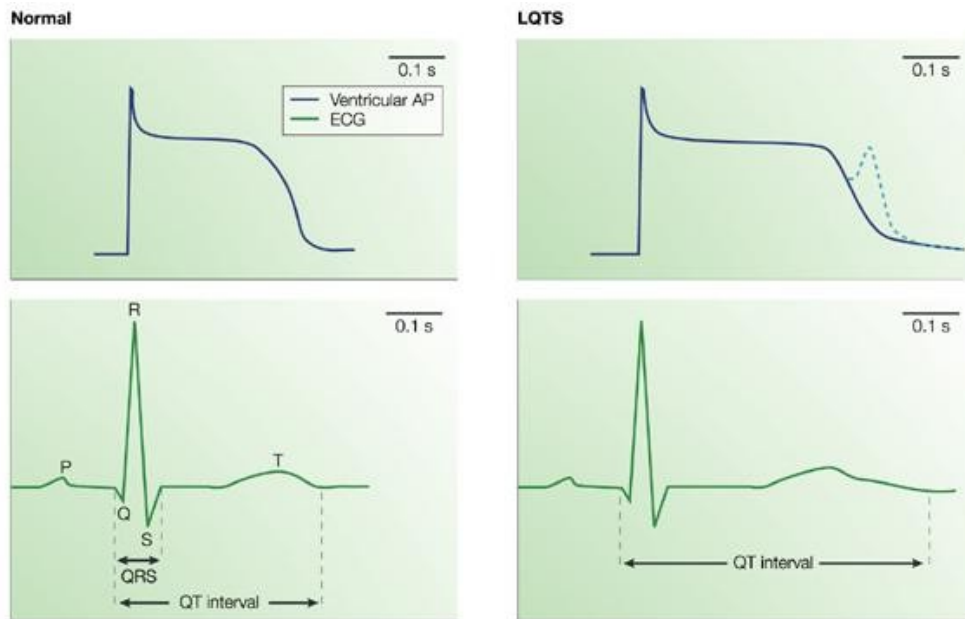


Figure 3: Illustration of action potential (AP) and Electrocardiogram (ECG) from normal subject and patient affected by Long QT Syndrome (LQTS). In LQTS, abnormalities in currents during the plateau phase of the AP (decreased repolarizing or increased depolarizing currents) lead to prolongation of the ventricular AP and hence the QT interval, as well as increasing the tendency for early after-depolarizations (dotted line), which markedly increases the risk of arrhythmias.

Presently, mutations in 13 genes involved in the correct execution of the cardiac action potential have been associated with LQTS. The functional effect of the mutation on the protein determines the type of the channelopathy [Hedley et al. 2009].

LQT-1 is the most prevalent genetic form of LQTS accounting for approximately 50% of genotyped patients. This type of syndrome is linked to KCNQ1 gene that encodes the α -subunit of the potassium channel conducting the I_{Ks} current, the slow component of the delayed rectifier current (I_K) the major repolarising current during phase 3 of the cardiac action potential.

LQT-2 is the second most common variant of LQTS accounting for 35%-40% of mutations. LQT2 is associated with mutation in KCNH2 gene that encodes α -subunit of the potassium channel conducting the I_{Kr} current the rapid component of the cardiac delayed rectifier [<http://www.fsm.it/cardmoc/>].

LQT-3 is linked to mutations in SCN5A gene, encoding cardiac sodium channel, and covers approximately 13% of all genotyped individuals with LQTS [Kies et al. 2004, Wang et al. 1996]. Most of these mutations are missense mutations, and are found to cause sodium channel gain-of- function, by disrupting fast inactivation and thereby causing an abnormal sustained (or persistent) non-inactivating sodium current [Priori et al. 2003]. Arrhythmic

events in LQT-3 usually occur at rest or during sleep when the heart rate is slow [Amin et al 2009].

LQT-4 is characterized by different phenotype: most of the affected individuals, besides QT interval prolongation, also present severe sinus bradycardia, paroxysmal atrial fibrillation (detected in >50% of the patients) and polyphasic T waves. LQT-4 is related with ANK2 gene that encodes Ankyrin B. This protein regulates the proper intracellular localization of plasmalemmal ion channels (calcium channel, sodium channel, sodium/calcium exchanger), sarcoplasmic reticulum channels (ryanodine receptor, inositol triphosphate receptor), and other adhesion molecules [<http://www.fsm.it/cardmoc/>, Bennett et al. 1995].

LQT-5 is associated with mutation in KCNE1 gene. The product of gene (minK) is the β -subunits of the potassium channel complex that produces the repolarizing I_{Ks} current in cardiac myocytes. Mutations in KCNE1 gene cause Jervell and Lange-Nielsen syndrome previously described [Mohler et al. 2003].

LQT-6 is linked to mutation in KCNE2 gene that encodes the β -subunits of the potassium channel complex that produces the rapid repolarizing I_{Kr} current in cardiac myocytes [Schulze-Bahr et al. 1997].

LQT-7 is associated to Andersen's syndrome (AS) that is a rare skeletal muscle disorder characterized by periodic paralysis, cardiac arrhythmias, and dysmorphic features. The candidate gene responsible of AS is KCNJ2 which encodes the inward rectifier potassium channel I_{K1} [Plaster et al. 2001, Tristani-Firouzi et al. 2002, Canùn et al. 1999].

LQT-8, known as Timothy Syndrome (TS), is a rare variant of LQTS characterized by marked QT interval prolongation and cutaneous syndactyly at both hands and feet. Severe prognosis has been observed in all cases described so far. All affected individuals show severe prolongation of the QT interval on electrocardiogram, syndactyly, and abnormal teeth and were bald at birth. The Arrhythmias were the most serious aspect of TS [George 2005]. The syndrome is caused by mutations in the $Ca_v1.2$ cardiac L-type calcium channel gene, CACNA1C [Splawski et al. 2005].

LQT-9 is linked to CAV3 gene which encodes Caveolin 3, the major scaffolding protein present in caveolae in heart. Mutations in CAV3 gene cause increasing in late sodium current (gain-of-function effect) [Vatta et al. 2006]. Caveolae are 50- to 100-nm omega-shaped microdomains of the plasmalemma, particularly abundant in cells of the cardiovascular system, including endothelial cells, smooth muscle cells, macrophages, cardiomyocytes, and fibroblasts. Caveolae are involved in vesicular trafficking and serve as a platform to organize and regulate a variety of signal transduction pathways [Westermann et al. 2005].

LQT-10 is caused by mutations in SCN4B encoding the sodium channel β -subunit Nav β 4. The mutation leads to a positive shift in inactivation of the sodium current, thus increasing sodium current [George 2009].

Recently, LQT-11 and LQT-12 were discovered; these two syndromes are caused by mutation in AKAP9 gene and SNTA1 gene respectively [<http://www.ncbi.nlm.nih.gov/>; MIM #192500].

1.4 Brugada Syndrome

The Brugada Syndrome (BrS) is a hereditary primary electrical disease, which is associated with right ventricular conduction abnormalities and coved-type ST elevation in the right precordial leads. Clinically, the syndrome is characterized by syncope and premature sudden death due to ventricular fibrillation [Wilde et al. 2002]. Arrhythmias in Brugada syndrome (and, thus, the symptoms) typically appear during predominant vagal activity, such as rest, or even during sleep [Miyazaki et al. 1996]. The syndrome is typically transmitted via an autosomal dominant inheritance pattern with incomplete penetrance. The prevalence of the pathology has been estimated at 5/1000 in Caucasians, although this figure possibly may be biased by the fact that it is currently not known whether a Brugada-like electrocardiogram always indicates the presence of the disease or it may be a non-specific finding in some cases. Therefore, the proposed figure may overestimate of the actual cases of BrS among the general population. [Hermida et al. 2000]. Patients usually present symptoms, especially SCD, during their fourth decade, although no conclusive explanation for this has been offered to date. Approximately 23% of the patients with SCD had already undergone syncope [Benito et al. 2008; Piori et al. 2002]. The disease is much more common in men than in women probably due to gender differences in the expression of the I_{to} and I_{Ca} , two currents involved in the phase 1 and 2 of cardiac action potential [Antzelevitch et al. 2003; Di Diego et al. 2002]. Great geographical variability has been reported, such that the syndrome seems to be much more frequent in Asia than in Western Europe or North America [Miyasaka et al. 2001; Wilde et al. 2002].

Three different ECG patterns related to Brugada syndrome were described: a) type I, characterized by a coved-type ST-segment elevation ≥ 2 mm in more than one right precordial lead (V1-V3), followed by negative T waves; b) type II, characterized by ST-segment elevation ≥ 2 mm in right precordial leads followed by positive or biphasic T waves, resulting in a saddle-back configuration; and c) type III, defined as any of the 2 previous types if ST-segment elevation is ≤ 1 mm (fig. 4). Although the 3 patterns can be observed in Brugada syndrome, and even in the same patient at different times, type I is the only one that is considered diagnostic of the disease. Thus, all patients who present a type I ECG pattern, even when isolated, should be considered at risk [Antzelevitch et al. 2005].

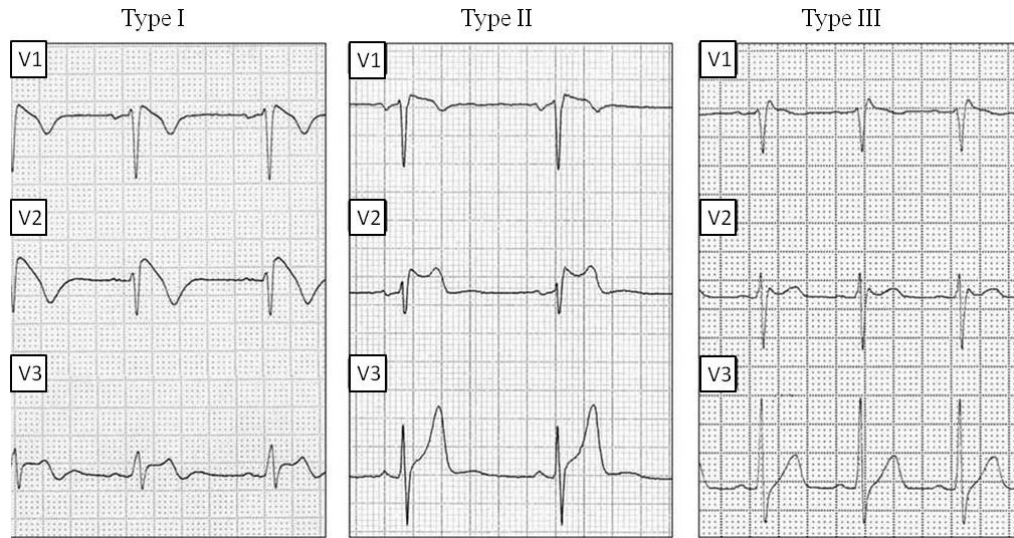


Figure 4: Electrocardiographic patterns (ECG) that can be found in the patients with Brugada syndrome.

This pathology is included among the so-called channelopathies, diseases produced by alterations in the transmembrane ion channels that participate in cell action potential, and which lead to an increased susceptibility to arrhythmias [Benito et al. 2009]. The first mutations associated with Brugada syndrome were found in 1998 in the *SCN5A* gene that encodes for the cardiac sodium channel. To date, more than 100 different mutations leading to Brugada syndrome have been described in the same gene but only 18% to 30% of the patients with Brugada phenotype show mutations in this gene, suggesting that the disease is genetically heterogeneous [Matsuo et al. 2003]. According to this hypothesis, 4 new genes associated with Brugada syndrome have been identified: *GPD1-L* (glycerol-3-phosphate dehydrogenase 1-like), *CACNA1c* and *CACNB2b* (encoding the calcium channel) and, quite recently, *KCNE3* (encoding β -subunit responsible for the transient outward potassium currents I_{to}) [London et al. 2007, Antzelevitch et al. 2007, Delpón et al. 2008]. Mutations in *SCN5A* gene, the alteration more frequent in Brugada syndrome, cause a decrease in I_{Na} , leading to an imbalance between the positive inward and outward currents at the end of phase 1 of the cell action potential [Vatta et al. 2002]. Similar situations occur when there is a decrease of the inward L-type calcium current (I_{Ca}) (produced by mutations in *CACNA1c* or *CACNB2b*) or an increase of the outward potassium currents (I_{to}) (produced by the mutation recently described in *KCNE3*) [Antzelevitch et al. 2007, Delpón et al. 2008]. Whichever the mechanism, the imbalance between the inward and outward currents leads to the development of a characteristic notch and the loss of the action potential dome mediated by an increase (relative or absolute) of

the outward I_{to} currents. Thus, since the density of I_{to} is greater in epicardium than in endocardium, this event occurs heterogeneously on the ventricular wall and leads to a transmural voltage gradient, which produces the characteristic ST-segment elevation in the ECG [Yan and Antzelevitch 1999]. The ion current imbalance at the end of phase 1 of the action potential also explains the susceptibility to develop ventricular arrhythmias in Brugada syndrome, which would arise via a phase 2 reentry mechanism [Benito et al. 2009].

1.5 Proteins Related to Long QT syndrome and Brugada Syndrome

1.5.1 Cardiac Sodium Channel

The cardiac sodium channel is a member of the voltage-dependent family of Na channels. These channels consist of heteromeric assemblies of an α -subunit, the pore-forming component, the function of which is modulated by association with one or two ancillary β -subunits.

The human cardiac sodium channel α -subunit ($Na_v 1.5$) is a heavily glycosylated protein of ~220 kDa consisting of 2016 amino acid residues [Tan 2006]. The protein is encoded by SCN5A gene that is located on chromosome 3p21 and consists in 28 exons [George et al. 1995]. The cardiac sodium channel generates the depolarizing current initiating the cardiac action potential and is crucial for the conduction of the cardiac impulse [Gallens et al. 1992]. This protein displays a modular architecture that consists of four internally homologous domains (DI-DIV) and each domain consists of six transmembrane α -helical segments (S1–S6), connected to each other by alternating extracellular and cytoplasmic loops (fig. 5A). The interdomain linkers and the N- and C- terminal ends of the channel protein are all located cytoplasmatically [Balsler 2001]. The four domains of the channel fold around a central ion-conducting pore, which is lined by the S5–S6 linker (referred to as the P-segment or P-loop) from each domain (fig. 5B). This loop, which exhibits a high degree of conservation among the various organ-specific isoforms across species, determines selectivity and conductance properties of the channel [Yellen et al. 1991]. In particular, the P-loops of domains III and IV play an important role in sodium selectivity. A lysine residue in the P-loop of DIII (K1418 in SCN5A), is critical for discrimination for sodium over calcium [Pérez-García et al. 1997]. The fourth transmembrane segment (S4), stereotypically studded with positively charged residues, functions as a voltage sensor and moves in response to depolarization, somehow opening the channel [Stühmer et al. 1989].

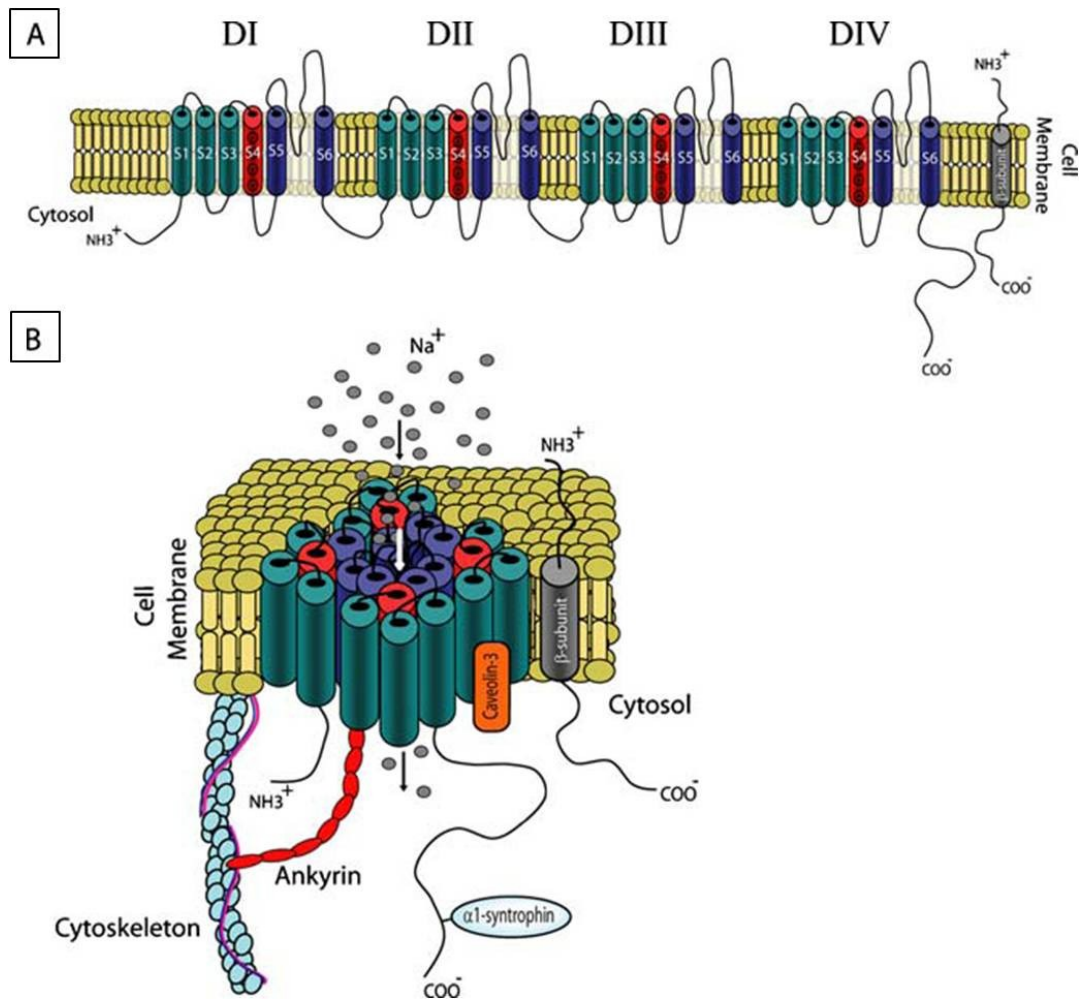


Figure 5: Voltage-gated cardiac sodium channel. A) Schematic bi-dimensional representation of cardiac sodium channel α -subunit and accessory β -subunit. B) Tridimensional representation of the four domains of cardiac sodium channel α -subunit folding around an ion-conducting pore and β -subunit.

The cardiac sodium channel differs from the neuronal and skeletal muscle isoforms in its sensitivity to block by tetrodotoxin (TTX). Whereas brain and skeletal muscle isoforms are blocked at nanomolar concentrations of TTX, the heart isoform is blocked at micromolar concentrations. Residues in the P-loop of DI are responsible for this isoform-specific difference in toxin binding [Satin et al. 1992].

Inactivation is characterized by at least two distinguishable kinetic components, an initial rapid component with a fast recovery time constant (fast inactivation) and a slower component with a slower recovery time constant

(slow inactivation). Fast inactivation is mediated, at least in part, by the DIII–DIV cytoplasmic linker [Stühmer et al. 1989]. This linker can be visualized as a hinged lid, which docks against receptor sites surrounding the inner vestibule of the pore, thereby occluding the pore. A critical component of DIII–DIV required for fast inactivation has been localized to the highly conserved hydrophobic triad IFM (residues 1485–1487 in the cardiac isoform). These residues are thought to interact with a receptor site that becomes available in the activated sodium channel [West et al. 1992]. The S4-S5 linkers in domains III and IV and residues on the cytoplasmic end of S6 of DIV could form part of this receptor site [Bennett et al. 1995; McPhee et al. 1995]. Structural determinants of slow inactivation are less known but are most probably localized within P-loops [Balsler et al. 1996]. Recent studies also suggest a role of COOH terminus in channel inactivation in brain and cardiac isoform [Cormier et al. 2002]. Recovery from the inactivated state occurs during repolarisation of the membrane during diastole.

In cardiac cells, $\text{Na}_v1.5$ associates with partner proteins, which may be anchoring/adaptor proteins, enzymes which interact with and modify the channel, and proteins modulating the biophysical properties of $\text{Na}_v1.5$ upon binding. $\text{Na}_v1.5$ also interacts with auxiliary β -subunits (~30–35 kDa, $\beta 1$ to $\beta 4$ -subunits) consisting of a small C-terminal cytoplasmic domain, a single transmembrane segment, and a large glycosylated N-terminal extracellular domain [Abriel & Kass 2005, Meadows & Isom 2005].

Sodium channels transit among various conformational states in the process of voltage-dependent gating. Depolarization from the resting membrane potential triggers activation (opening) of the Na channels. If the depolarization is maintained, the channels enter a non-conducting inactivated state. Subsequent to repolarization, the channels return to a closed state capable of being activated once again. It is becoming increasingly clear that these processes are the results of complex allosteric interactions among many structural domains of the channel [Meadows & Isom 2005].

1.5.2 Potassium Channels

Voltage-gated K^+ channels are membrane-spanning proteins that regulate potassium ion movement across the cell membrane. They are important in maintaining electrical activity in most excitable cells because they control cellular resting potential and action potential duration. Potassium channels are highly regulated and are the basis for the change in action potential configuration in response to variation in heart rate. Because of the uniquely slow voltage–time course of the cardiac action potential plateau, there is particular physiological relevance of K^+ activation kinetics, channels with slow or “delayed” and these channels have been referred to as “delayed” rectifier channels [Bezzina et al. 2001; Noble and Tsien 1969]. Two components of potassium-selective activated during prolonged depolarization in the plateau voltage range. The delayed rectifier potassium current is a voltage- and time-

dependent K^+ current with two components that can be separated on the basis of activation kinetics and pharmacology: a rapidly activating current called I_{Kr} and a slowly activating component called I_{Ks} . The delayed K^+ , I_K , current were generated by HERG 1 (I_{Kr}) and K_vLQT1 (I_{Ks}) channels [Sanguinetti and Jurkiewicz 1990].

1.5.2.1 HERG: Rapid Rectifier Delayed Potassium Channel

The rapid delayed rectifier K^+ current, I_{Kr} , plays an important role in normal repolarization of cardiac action potential. The I_{Kr} is conducted through channels complex formed by tetrameric assembly of human ether-a-go-go-related gene, HERG and one ancillary β -subunit [Morais Cabral et al. 1998]. In humans, HERG protein is encoded by *KCNH2* gene, which is located on chromosome 7q35-36, and the coding region comprises 16 exons spanning approximately 34 kb of genomic sequence. The full-length HERG1 subunit (hERG1a) is composed of 1159 amino acids with a molecular mass of 127 kDa [Dennis et al. 2007]. The gene encodes the α -subunit of the rapid delayed rectifier current I_{Kr} in the heart. The HERG channel has the same body plan as that of other voltage-gated ion channels. HERG subunit has six transmembrane α -helices, with the fourth one (S4) carrying seven positive charges distributed at every third or fourth position and a reentrant "pore-loop" between the fifth and sixth transmembrane helices (fig. 6) [Doyle et al. 1998].

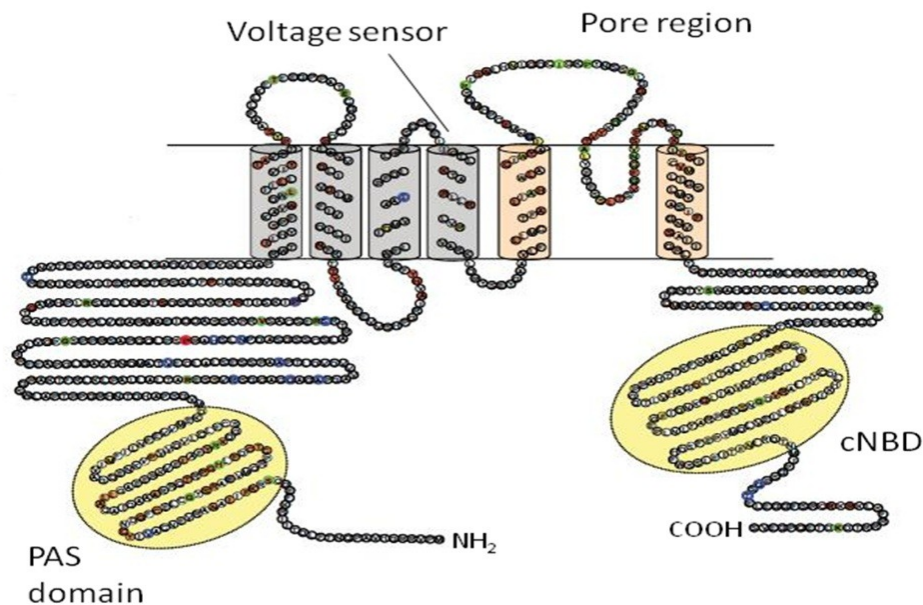


Figure 6: Schematic representation of rapid delayed rectifier potassium channel HERG.

HERG1a has a long N-terminus (376 amino acids) and residues from 1 to 135 comprise the so-called “eag domain” that is protein-protein interaction structure called a Per–Arnt–Sim (PAS) domain [Sanguinetti et al. 1995]. The function of the PAS domain in hERG1a is uncertain; however, LQTS-associated mutations in this region disrupt channel trafficking and accelerate the rate of deactivation, perhaps by disrupting its interaction with the S4–S5 linker of the channel [Chen et al. 1999; Wang and Trudeau 1998]. The PAS domain can be phosphorylated and needs to be properly folded for normal trafficking of the channel complex from the endoplasmic reticulum to the Golgi and cell surface [Cayabyab and Schlichter 2002; Paulussen et al. 2002]. An alternatively spliced variant of hERG1 (hERG1b) was isolated from mouse and human heart and is composed of 819 amino acids with a predicted molecular mass of 94 kDa [Lees-Miller et al. 1997; Jones et al. 2004]. The N-terminus of hERG1b is only 36 amino acids and lacks the PAS domain but has an “RXR” ER retention signal sequence that prevents its trafficking to the surface membrane unless coassembled with hERG1a subunits [Phartiyal et al. 2008]. Both HERG1a and HERG1b show a long C-terminus that contains a cyclic nucleotide binding domain (CNBD). HERG1 proteins can coassemble with ancillary β -subunits called MiRP1 (encoded by KCNE2 gene) [Abbott et al. 1999]. A reduction of I_{Kr} caused by LQTS-associated mutations in KCNH2 can induce ventricular arrhythmia and cause sudden cardiac death [Schwartz and Bauer 2004].

1.5.2.2 KCNQ1: Slow Rectifier Delayed Potassium Channel

In cardiac myocytes, the KCNQ1 subunit assembles with the KCNE1 β -subunit (minK) and forms a channel complex constituting a very slowly activating voltage-gated current, closely resembling the cardiac delayed rectifier current I_{Ks} which is partly responsible for terminating the cardiac action potential [Abbott et al. 1999]. KCNQ1 potassium channels are expressed in several tissues throughout the body and regulate key physiological functions. The two most important roles of KCNQ1 channels are 1) repolarization of the cardiac tissue following an action potential and 2) water and salt transport in epithelial tissues [Barhanin et al. 1996].

KCNQ1 gene is located on chromosome 11p15.5 and consists in 15 exons [Neyroud et al. 1999]. The gene is expressed in many different tissues, mainly heart, pancreas, kidney and intestine [Yang et al. 2002]. The primary translated protein (isoform 1) consists of 676 residues and has six transmembrane domains, a pore loop with a typical potassium-channel pore-signature sequence (GYGD), and intracellular NH_2 and $COOH$ terminals, covering 122 and 322 residues, respectively. The S4 segment contains numerous positively charged amino acids and plays a role as a voltage sensor for voltage dependent activation kinetics (fig. 7) [Lee et al. 1997]. Six different splice variants (isoforms 0–5) of human KCNQ1 have been reported. Isoform 1, described above, and isoform 2, encoding translational start in the middle of membrane

segment 1, are, when detected at the mRNA level, the two major splice variants found in the heart. When expressed in a heterologous context, the isoform 2 protein functions as a dominant negative isoform [Wang et al. 1996]. KCNQ1 is a typical K^+ channel α -subunit of that consists of six transmembrane domains and a pore-forming region, and belongs to the rapidly expanding family of KCNQ-channels whose members are widely expressed in epithelial and excitable cells [Takumi et al. 1988]. KCNQ1 gene product is very important also for the normal function of the inner ear as exemplified by Jervell and Lange-Nielsen syndrome that is associated to recessive loss-of-function mutation found in this gene causing deafness with severe QT prolongation [Jervell and Lange-Nielsen 1957].

I_{Ks} current is mediated by β -adrenergic receptor activation, leading to an increased level of cAMP and thereby PKA stimulation, which interacts with the I_{Ks} complex through an A-kinase anchoring protein (AKAP) (fig. 7) [Potet et al. 2001].

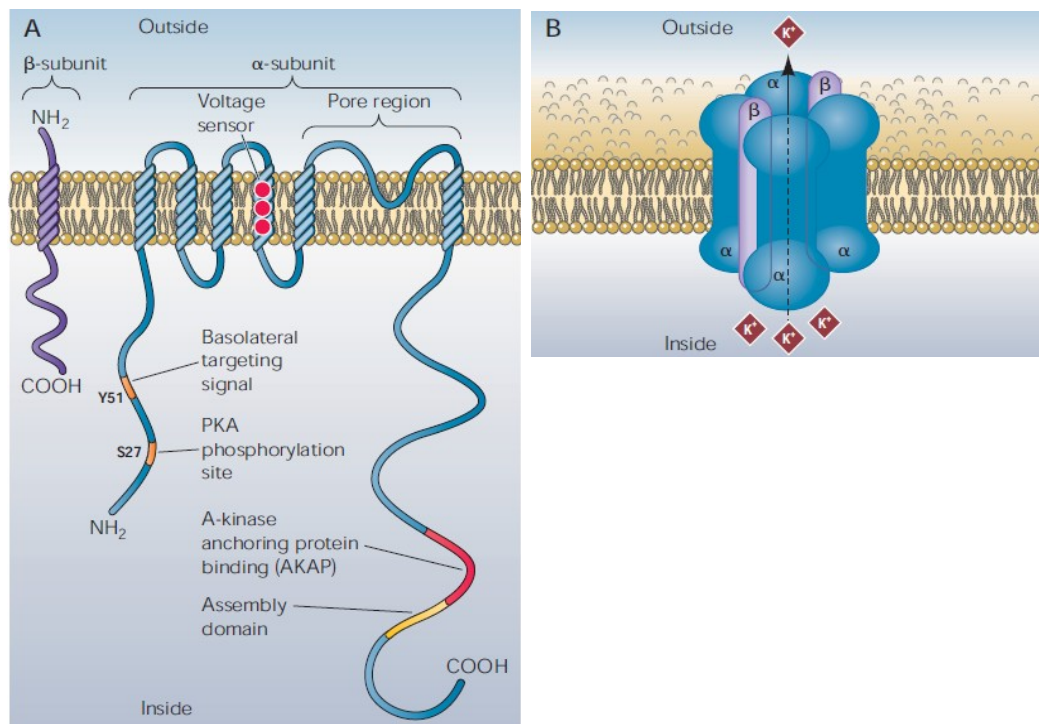


Figure 7: Slow rectifier delayed potassium channel. A) Schematic bi-dimensional representation of KCNQ1 (α -subunit), with interacting domain, and MinK1 (β -subunit). B) Representation of tetrameric complex of α -subunits with ancillary β -subunits.

PKA and protein phosphatase 1 interact with KCNQ1 through the AKAP called yotiao, which binds to the COOH-terminal tail of KCNQ1 via a leucine zipper. Upon PKA activation, residue S27 in the NH2 terminal of KCNQ1 is phosphorylated. However, yotiao seems not only to be important for mediating the phosphorylation of S27, but it is also necessary to transform the phosphorylated KCNQ1 subunit into a channel with altered activity. The cAMP-mediated regulation of KCNQ1 channels in mammalian expression systems is dependent on coexpression of KCNE1 [Kurokawa et al. 2004]. Phosphatidylinositol-4,5-bisphosphate (PIP2) is another key intracellular regulator of the KCNQ1/KCNE1 channel activity. PIP2 affects the IKs channel by stabilizing the open state [Park et al. 2005].

The voltage-gated KCNQ1 channel is progressively opened by increasing membrane depolarizations. The channel gives rise to slowly activating and deactivating potassium currents [Franqueza et al. 1999]. Upon longer depolarizing steps a fraction of the KCNQ1 channels inactivate [Push 1998].

1.5.3 MirP and Mink

MiRP1 (MinK-related peptide 1) is a small integral membrane subunit that forms stable assemblies with HERG channel. The protein is encoded by KCNE2 gene and consists in 123 residues, with two N-linked glycosylation sites a single transmembrane segment, and consensus sequences for two protein kinase C-mediated phosphorylation sites (fig. 8). MiRP1 regulates HERG in vitro, accelerating its deactivation 2–3 fold and reducing unitary conductance 40%. Missense mutations in the gene for MiRP1 are associated with inherited and acquired arrhythmia and changes in channel function [Abbott et al. 1999].

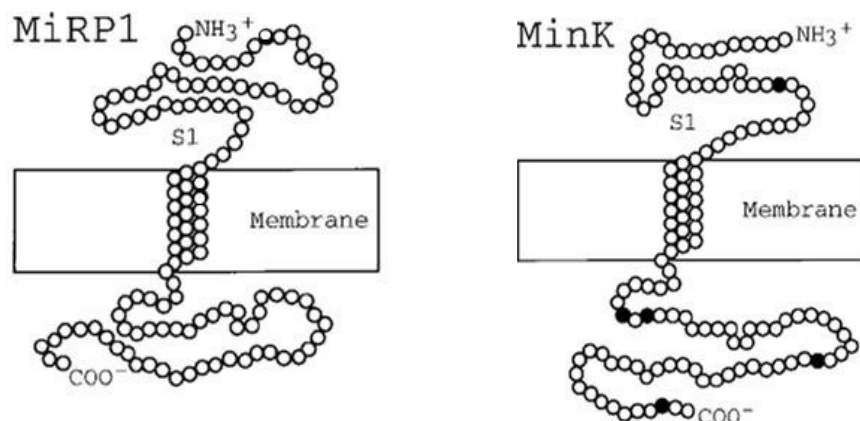


Figure 8: Schematic representation of the ancillary β -subunit *MirP1* and *MinK*.

Chapter 2

TECHNICAL BACKGROUND

2.1 Why the Patch Clamp?

2.1.1 Basic Information

Electrical excitation of the heart is accomplished by the generation and propagation of cellular action potentials, which is a change in voltage over time. The action potential results from the flow of ionic currents across cell membranes [Kornreich 2007]. In addition to containing many conducting channels, the lipid bilayer of cellular membrane separates internal and external conducting solutions by an extremely thin insulating layer. Thus, the membrane, considered as a narrow gap between two conductors, forms a significant electrical capacitor [Hille 2001]. The cell membrane is so thin that charges are attracted to one another across the membrane, with negative charges accumulating near the interior surface of the membrane and positive charges near the exterior surface [Kornreich 2007]. The measure of how much charge needs to be transferred from one conductor to another to set up a potential difference between them is defined as capacitance (C), measured in farads (F) [Hille 2001]. The alignment of charge along the membrane is sufficiently uniform that the capacitative charge is a reliable index of membrane area and, therefore, of cell size [Kornreich 2007].

Ion channels on the cellular membrane play a key role in initiated and propagating the action potential. The most powerful techniques available for studying functional aspects of voltage-gated ion channels is the voltage clamp. The principle of the method is to isolate a patch of membrane electrically from the external solution and to record current flowing into the patch. Changes in voltage, produced by this technique, induce channels to interconvert between different states, and these transitions are monitored as changes in membrane current. The voltage clamp can be used to activate different populations of channels selectively. In this way, a specific channel targeted by biological or pharmacological manipulations can often be identified and studied in detail [Crawley 1997].

Biological electrical activity results from the separation and movement of charged particles, typically cations such as Na^+ , K^+ and Ca^{2+} . Charge is usually separated by a lipid membrane and the movement of charge across the

membrane requires: a driving force and a path for current flow. The movement of charge is defined as current (I), measured in Amperes (A), whereas the driving force, measured as the work needed to move charge from one point to another, is termed voltage (V), measured in Volts (V). The path for current flow most often is an ion channel and the ease with which charge moves through the channel is resistance (R), measured in Ohms (Ω). The relationship between V, I and R is defined by Ohm's Law: $I=V/R$; where it is apparent that the larger the voltage, the larger the current and similarly, the smaller the resistance, the larger the current. If the voltage across a membrane is held constant, increasing, or reduction, in current will be directly associated with changes in resistance. This relationship provides the basis for the voltage clamp technique, where the voltage is held at a constant value and current is measured at that voltage. In an actual voltage clamp experiment, the resistance in the voltage clamp circuit is not determined solely by ion channel resistance. Rather, the total membrane resistance also must be considered [Kornreich 2007]. The measure of the ease with which current flows through an ion channel often is represented by the reciprocal of resistance, or conductance (G), measured in Siemens (S). This parameter is a basic biophysical property of an ion channel, given that in most cases the opening of an ion channel is an "all or none" phenomenon. Using Ohm's Law, conductance of an ion channel can be described as: $G=I/V$ [Hille 2001].

2.1.2 The Patch Clamp Technique

The patch clamp technique is an ideal methodology for investigating the molecular mechanisms of cardiac electrical activity under both physiologic and pathologic conditions. In fact, the patch clamp recordings have the ability to monitor electrical activity at the level of the individual ion channel in the context of cellular membrane. Studies of the electrical properties of biological membranes can be subdivided roughly into extracellular recording and intracellular recording techniques. Intracellular recordings measure the difference in voltage or current across a cell membrane, whereas extracellular recordings measure differences in these parameters within the extracellular space. Intracellular recording of transmembrane current during a holding transmembrane voltage at a value is referred to as voltage clamp, whereas the measurement of transmembrane voltage while holding transmembrane current at a determined value is termed current clamp. Several configurations of the voltage clamp technique have been developed (fig. 9). These configurations vary with respect to membrane integrity, membrane orientation, and continuity between the intracellular space and intrapipette solutions [Kornreich 2007].

One of the features that makes the patch clamp that so powerful is that it can be used in different configurations, which enables the experimenter to study ion channels at different levels and manipulate easily the fluid on the extracellular or intracellular side of membrane during recordings [Molleman 2002]. Depending upon which configuration is used, the electrical activity of

either single ion is used, the electrical activity of either single ion channels (single channel), the ensemble activity of a large number of channels within a small patch of membrane (giant patch), or the activity of all channels within a cell (whole cell, perforated patch, sharp electrode) may be measured.

The majority of these techniques involve the initial formation of a high resistance gigaseal between the tip of the recording pipette and the cell membrane. This high resistance seal, discussed previously, prevents the passage of ions between the pipette and the membrane [Kornreich 2007].

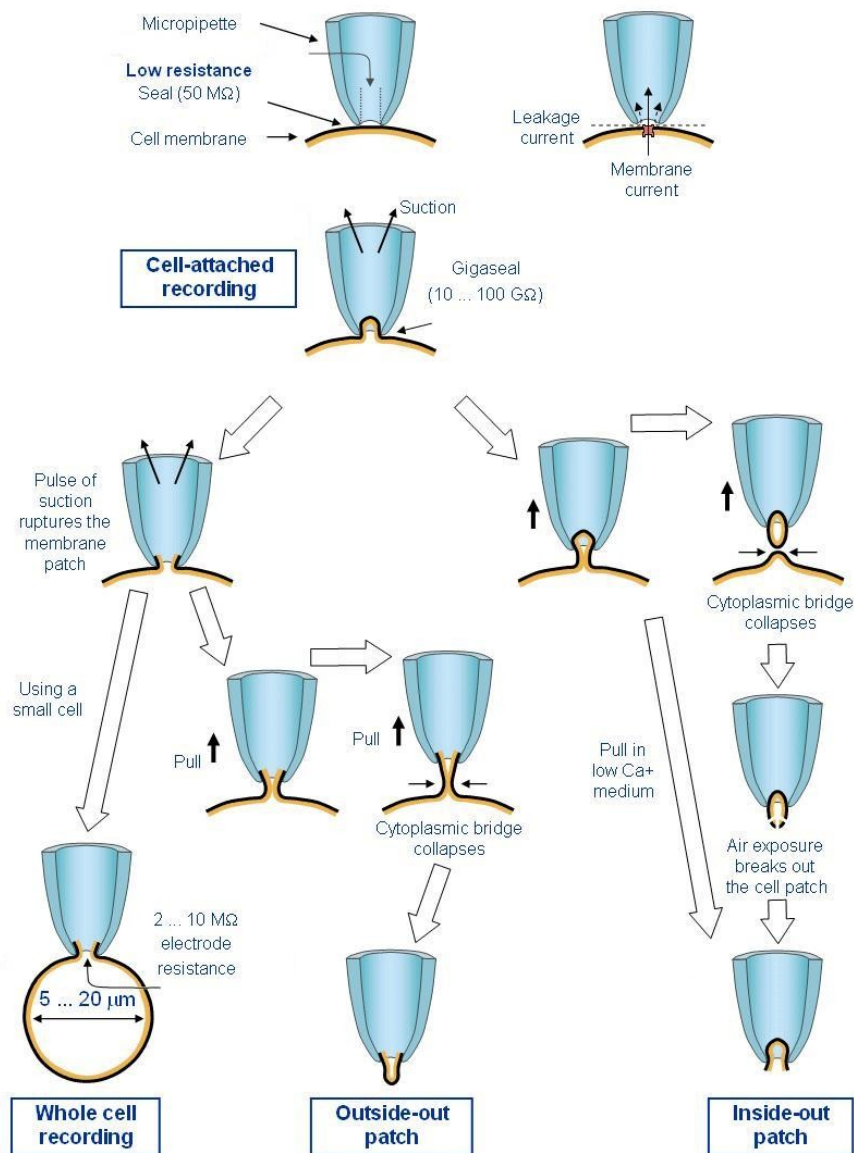


Figure 9: Representation of various configurations of the patch clamp technique and description of how to obtain them.

2.1.3 Whole Cell Patch Clamp Configuration

The whole-cell voltage clamp was an offshoot of the patch-clamp technique, which originally was designed for measuring current through single channels. In the early uses of the patch clamp, the voltage across a small patch of membrane on the surface of a cell was clamped by a glass micropipette (named also pipette or electrode) with a tip of $\sim 1 \mu\text{m}$ in diameter; hence the term patch electrode [Heinemann 1995]. Subsequently, it was found that the patch of membrane under the electrode tip could be removed, and once this happened the electrode attained direct electrical contact with the cell interior. As a result, the voltage across the entire cell membrane was clamped instead of the voltage across the tiny patch, so this technique was named as whole-cell patch clamp [Crawley 1997].

The whole cell patch configuration is obtained by applying negative pressure or a short duration, high voltage pulse to the recording pipette after attaining the cell attached configuration. This manipulation breaks the patch of membrane inside the tip of the electrode, thereby making the intracellular space contiguous with the internal pipette solution. In electronic terms, this implies that patch resistance (R_{patch}) becomes very low and, such as, is usually renamed access resistance (R_a). The membrane potential is disrupted as the integrity of the plasma membrane is lost and the pipette has direct contact with the cytoplasm [Molleman 2002]. Figure 10 shows the equivalent electric circuit of whole-cell patch clamp configuration.

Following, dialysis of the internal pipette solution into the cell occur; the composition of the intracellular space and the internal pipette solution equalize. A single electrode (pipette) allows both to control voltage and measure current.

Thus, the whole cell configuration allows the study of the ensemble response of all ion channels within a cell's membrane. An additional benefit of whole cell recordings is that compounds can be diffused into the intracellular space and their effects on ion channel function quantified. However, one potential pitfall of the whole cell configuration is that components of the intracellular milieu can diffuse out of the cell into the patch pipette, in some cases with significant effects on ion channel function [Kornreich 2007].

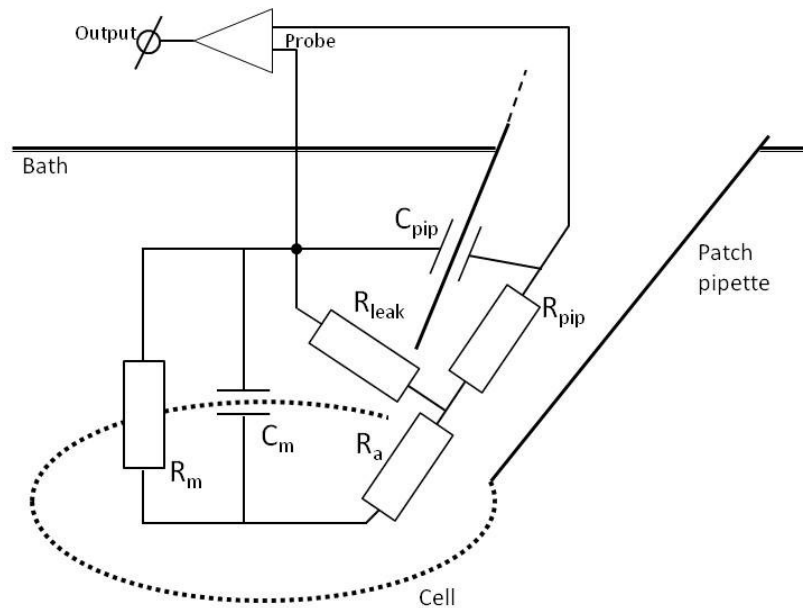


Figure 10: Equivalent electric circuit for the whole-cell patch clamp configuration. The dotted line represents the cell membrane. R_m = membrane resistance, C_m = membrane capacitance, R_a = access resistance, R_{pip} = pipette resistance, C_{pip} = pipette capacitance, R_{leak} = leakage resistance.

The principle of the method is to isolate a patch of membrane electrically from the external solution and to record current flowing into the patch. This is achieved by pressing a fire-polished glass pipette, which has been filled with a suitable electrolyte solution, against the surface of a cell and applying light suction [Crawley 1997]. A key characteristic of an electrode is its resistance when filled with the patch-electrode filling solution. The resistance provides a useful indicator of the electrode tip size [Sakmann 1995].

The technique depends on the ability to form a tight seal between the electrode tip and the plasma membrane of a cell targeted for study [Crawley 1997].

Providing both glass pipette and cell membrane are clean, a seal whose electrical resistance is more than $1 \text{ G}\Omega$ is formed, known as “gigaseal”. The higher the seal resistance, the more complete is the electrical isolation of the membrane patch and high seal resistance reduces the current noise of the recording, permitting good time resolution of single channel currents. The achievement of gigaseals, however, radically improved the quality of recording and made it possible to study channels of lower unitary conductance [Sakmann 1995].

The conditions that appear to be required for the formation of a gigaseal are the following:

- First, the surface membrane of the cell used must be clean and free of extracellular matrix and connective tissue. Cells in tissue culture are often preferred; adult cells generally must be cleaned enzymatically or mechanically.
- Secondly, solutions should be free of dust and of macromolecules such as the components of serum in tissue culture media. Solutions are filtered using 0.2 μm filters. Cell cultures are washed several times to remove serum.
- Thirdly, the pipette tip should be clean, often by fire-polishing.
- Fourthly, during the period just prior to seal formation, a small positive pressure is applied to the pipette to generate an outflow of solution from the pipette tip and so keep it free of debris [Ogden & Stanfield 1994].

2.1.4 Fabrication of Patch Pipettes

Two important technical concerns associated with the formation of a gigaseal are cleanliness of the system and the composition and geometry of the patch pipette. In order to eliminate particulates and other impurities that may interfere with seal formation, all solutions are filtered (usually through a 0.22 micron filter) prior to their use in experiments. In addition, pipettes are pulled from borosilicate glass capillary tubes as close to the time of their use as possible and are kept in a sealed chamber to prevent airborne particulates from contaminating their tips. Borosilicate glass is used in this application because of its relatively low electrical noise (which is a function of its dielectric constant), low softening temperature (which promotes ease and success of pipette pulling), and the ease with which it forms high resistance seals with cell membranes. It is important to lower the pipette into the bath solution as rapidly as possible and to apply positive pressure to the internal pipette solution to avoid contamination of the tip of the pipette with impurities that may be floating on the surface of the bath [Kornreich 2007].

2.1.5 Patch Clamp Protocols

Typically, it is most useful to record one particular type of ionic current at a time. Two general strategies can be used to isolate the current of interest:

- First: all currents other than the current of interest are blocked using specific ion channel blockers, elimination of the ion that carries a particular current (e.g., removal of sodium ions to block sodium current) or the delivery of voltage clamp protocols that either fail to activate or inactivate the unwanted current(s).
- Secondly, measurements are initially made of the total cellular current, after which the cell is exposed to a drug that selectively blocks only the current of interest. The current records obtained before and after exposure to the blocker are subtracted from one another, yielding a “subtraction current” that should be a faithful replicate of the current of interest.

The activity of specific ion channels may be studied individually or they may be studied as part of an ensemble response in a whole cell configuration.

Isolation of a specific voltage gated ion channel's activity may be achieved by using rationally designed voltage clamp protocols (fig. 11), ion channel blockers, by expressing desired channel proteins in a system lacking other ion channels, or by a combination of these methods. Studying an isolated ion channel's activity can provide important information regarding voltage sensitivity of activation, inactivation, and recovery from inactivation, as well as the effects of drugs on channel function [Kornreich 2007].

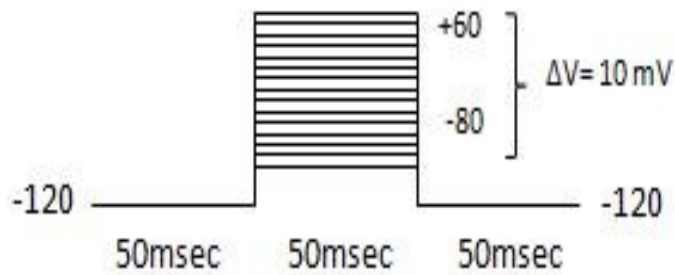


Figure 11: Voltage clamp protocol used to activate the cardiac sodium channel. Fifteen depolarizing steps from -80 mV to +60 mV in 10-mV increments from holding potential -120 mV were applied in this protocol.

Chapter 3

AIM OF THE STUDY

The aim of the study was the determination of genotype-phenotype correlation in Southern Italy patients affected by long-QT syndrome or Brugada syndrome.

Our goal was to determine the molecular basis of cardiac arrhythmias including long-QT syndrome and Brugada syndrome. We proposed to elucidate the biophysical properties of cardiac ion channels mutations to well understand the pathogenesis of these syndromes. To functional characterize the cardiac ion channel mutants we carried out electrophysiological studies to identify biophysical defects that can be the trigger for the long QT or Brugada syndrome phenotype.

In order to reach our goal we firstly used dHPLC and automatic sequencing to perform the molecular analysis in SCN5A, KCNH2, KCNQ1, KCNE1 and KCNE2 genes. Afterward, we functional characterized the novel mutation by patch clamp technique in whole-cell configuration.

This work was performed at Department of Biochemistry and Medical Biotechnologies (DBBM) and CEINGE-Advanced Biotechnology. Furthermore, the electrophysiological experiments were carried out at the Vanderbilt University (Nashville, TN, USA), Medical Center at the Department of Medicine and Pharmacology, Division of Molecular Genetics in the laboratory of Prof. Alfred L. George.

Chapter 4

MATERIALS AND METHODS

4.1 Patients and Control Population

Forty-nine unrelated patients showing LQTS phenotype and fifty-four showing BrS phenotype were enrolled in genetic study. The genetic analysis was also carried out on the patients' relatives. All affected subjects came from Southern Italy. Informed consent to perform genetic analysis was obtained from each patients according to the procedure established by Italian law and by ethics committees of the participating institutions.

The control population consisted of 200 anonymous, healthy Caucasian individuals, whose DNA samples were donated by the Biological Sample and Cell Bank of CEINGE (CEINGE s.c.ar.l.–Biotecnologie Avanzate, Naples, Italy).

The molecular analysis was performed in 4 steps:

- 1- DNA extraction;
- 2- Amplification of 85 amplicons of SCN5A, KCNH2, KCNQ1, KCNE1 and KCNE2 genes by PCR;
- 3- Analysis of PCR products by dHPLC
- 4- Automatic sequencing of exons showing abnormal elution profile (different elution profile from WT).

4.2 Genomic DNA Extraction and PCR

Genomic DNA of each subject was extracted from 5 mL of peripheral whole blood using Nucleon BACC2 Kit (Amersham Biosciences, UK). All coding exons (included splice site regions), 5' UTR and 3' UTR of SCN5A, KCNH2, KCNQ1, KCNE1 and KCNE2 genes were amplified by polymerase chain reaction (PCR). All primers used in PCR procedure were designed by Primer 3 program (<http://frodo.wi.mit.edu/primer3/>). Amplification conditions were listed in tables 1, 2, 3 and 4.

Table 1: PCR and dHPLC conditions of SCN5A exons.

Exons	Forward primer (5'→3')	Reverse Primer (5'→3')	PCR T _a (°C)	Product Size (bp)	dHPLC T (°C)
1	gggtcagtgtagtg	ctcggggaggaaagtgg	59	456	68, 69
2	gtccctgggcatagaatcag	gtaggcagggtgaggt	59	398	61, 63
3	tctcctcctccacctc	taggaccagcaggaatcag	59	356	60, 61
4	ggagaccctgtttattgtctgg	ggcatggaatggaaggaa	59	271	61, 62
5	ccacgtaaggaaactggaga	aggaggaaagccagaaagag	59	308	60, 62
6	tggtgtgtgtcattgtctcg	gagccctgggaaaggtattc	59	264	58, 59
7	ccacccagctcaactca	gctggtctcacaagtcttcc	59	398	61, 62
8	aggggcagagaagaaggag	tggggtcagggcataaatag	59	278	60, 61
9	actgagctgtgggcataaa	tgttagcctggaccctga	59	312	62, 63
10	gaaccctggcacaactaga	agttaggtgaggcttagagg	59	337	61, 62
11	gaggctgcacaaagtctcaa	cagaccaccctggaaaag	59	275	60, 61
12A	gctgggagcacatgaagag	accattgcagtcaca	59	339	61, 62
12B	gcagatgatgaaacagcaca	atcttggacttgccactgg	59	337	63, 64
13	ccagtgtccatcaagacct	tcaggctgggataaagatgag	59	346	63, 64
14	tcagtcaacagaatcaaactaactca	aggatgccatttgagagc	59	370	61, 63
15	ctgccacagcaagagtcaag	gggatgaccaagtgatgacc	58	345	61, 63
16A	gctttcaggcaggagctaga	agatgatgaggaaaggcatga	59	331	61, 62
16B*	cggttcatctttgctgtgg	gggtgggtagctgggtgat	59	298	-
17A	ccccatcatagaactgggact	tgctgccttctcaaac	59	386	61, 62
17B	attgccacccctactcc	gccttctaccctaccact	TD 65-58	349	61, 63
18	catgggcagggtctgaaa	ggctccaacagcaaatg	59	350	62, 63
19	tgctactcagcccactca	ggtcacagaggaatggagga	59	321	62, 63
20	tagatgtggcattcagag	ccccatttctgacctgactt	TD 65-58	313	62, 63
21	gtggaatcggcagtggtc	gcaatgggtttctccttct	TD 65-58	274	62, 63
22	accgtcttagtggaccaga	cataggacatcagaagcacagg	TD 65-58	314	61, 62
23	ggtcttgaagggcatgtg	aacagccattgggaggaag	59	391	60, 61
24	gcttctggcttcatctgtcc	gcagacactgattccctggt	59	229	58, 59
25	tagacagccctctgcctctg	aggtgagatgggacctgga	TD 65-58	326	58, 61
26	atcctggcatcctcatcaag	ctgggctgaaagactgtgaa	59	311	60, 61
27	tgagaggcagcaacaggcatt	ctggctggggagggtcttct	TD 65-58	390	59, 60
28A	atgctggctggaagacagag	ggcgaaggctggaattg	59	339	60, 61
28B	tctactccatctttggcatgg	ggccacgctaagttctc	59	326	60, 61
28C	tctcctcctcatctgtgtc	atcttcagggtcctcatct	59	346	60, 61
28D	cattctcttgcctcaccaa	caaggggtcgggagaagt	59	326	61, 62
28E	aagaggatgccctgagc	caggctggtttgtgactga	59	325	62, 63
28F*	ccaggacacactgaaaagca	gaaagccattcacaacatataca	59	302	-
28G*	ggctctggaaagcaactca	gtgtgtgtcctgtgtgagtg	59	340	-
28H	ccacttgacctgagatgctg	gaggggaagaaaaggcaac	59	326	60, 63
28I	ggctccagaggagagtg	aggagctggagaccacacag	59	340	60, 63
28L	gcctgaagagaggaaactgg	gcctttcacaagacctatgg	59	321	62, 63
28M	atggcaccacacagagg	gcactgccacaaatgtcc	59	365	58, 59
28N	gctggctgctcctaacctac	aaccgattcctgcctgt	59	339	59, 60
28O	agaggatgtgccctcct	agcacaaggacagagcctaga	59	406	59, 60

The table shows the number of exons, primers sequences, annealing temperature (T_a), product size (bp) and dHPLC temperature (dHPLC T).

The bold sequences represent primer that anneal with coding sequence; TD= Touchdown PCR; *= exons analyzed only by automatic sequencing.

Table 2: PCR and dHPLC conditions of *KCNH2* exons.

Exons	Forward primer (5' → 3')	Reverse primer (5' → 3')	PCR T _{An} (°C)	Product Size (bp)	dHPLC T (°C)
1*	ggcccccgaagcctagtgc	Attgactcgacttgccgac	TD 65-58	266	-
2*	tgtgagtgagaatgtgggaag	Tctgaccccccttggtc	TD 65-58	361	-
3	tgcccactgagtggtgc	Tgacctggacagctcacag	64	288	61, 62
4:01	acgaccagtgcctctcctctc	Gggaccaccagcgacgccc	64	267	67, 68
4.2*	ccctggacgaagtacacccatgg	Ggctggggcgaacgggtcc	TD 65-58	319	-
5	ggcctgaccacgctcctct	Ccctctcaagctctccaa	TD 70-60	293	62, 63
1B	ggtgcaggtgaggcagtg	Cggccccagaaagaaggaa	TD 70-60	232	64, 65
6	gtccatggcctgcctcacc	ctacaccactgcctctgctgac	64	533	62, 63
7	tgcccatcaacggaatgtgc	Gccgccccctgggcactca	64	449	61, 62
8	ctgacctggtcggggcctg	Cccagctgccaccact	64	327	64, 65
9	ccaaggagggtgtgctgag	Ggcatttcagctccagtgc	64	331	64, 65
9 USO	agcactgcaaacccttccgag	Tagtgaaccaaatgccgagc	TD 70-60	598	62,5, 63,5
10	ccccgggctgagctccctgctc	Tccagctcaggcagccaa	64	257	62, 63
11*	agagcactgaaagggcctga	Ggtctgaggcctggtaaagca	TD 65-58	239	-
12*	tcccctctgagggccattc	Ggggtagacgcaccaccgct	TD 65-58	370	-
13*	ctgaccagctctgctctctg	Caccaggacctggaccagact	TD 65-58	273	-
14	atcccggaggaggctgtca	Gaacaagcgggcccaggtac	64	287	62, 63
15	tgccatgctctgtgtattg	Acgtgtccacactgggcag	64	199	60, 62

The table shows the number of exons, primers sequences, annealing temperature (T_a), product size (bp) and dHPLC temperature (dHPLC T). TD= Touchdown PCR; *= exons analyzed only by automatic sequencing.

Table 3: PCR and dHPLC conditions of *KCNQ1* exons.

Exons	Forward primer (5'→3')	Reverse primer (5'→3')	PCR T _a (°C)	Product Size (bp)	dHPLC T (°C)
1A	tcgccttcgctgcagctc	tccccacaccagctctcag	TD 70-60	510	65, 66
1B	cccctgctctcaccacaa	tctaccgccaccataact	TD 70-60	209	62, 63
1	ctacctggggcggggctga	gtgtgggcaaggggctggga	TD 65-55	310	63, 64
2	aggcatcaccatccgagca	tgctcctgtgctgggtcctg	TD 70-60	435	62, 63
3	cccttcccagacgagagca	ctccaccatcccagcacat	TD 70-60	330	63, 64
4	aggggcaggggcagggacac	cggggcctcagcgcattca	TD 70-60	300	64, 65
5	tcgtgggactcgtgcctt	tgtcctgcccactcctcagcct	TD 70-60	291	63, 64
6	gggtttgggttaggcagttgg	agccaccccaggaccccag	TD 70-60	247	63, 64
7	tggcctgtgtggacggga	cagtgacaaaatgacagtga	TD 70-60	179	62, 63
8	gggaacagggagggggagct	ggcctccccactgctagca	TD 70-60	266	60, 62
9	ctgggctcggggcggtg	ctctgtctgttcatacctcgtt	TD 70-60	367	57, 60
10	ctggcaggttgggtgggagg	aggcagacggcaagtgggtg	TD 70-60	310	61, 62
11	caggggcagtgagggatga	gtggcttggggcgagg	TD 70-60	270	62, 63
12	cactgcctgcactttgagcc	gtgaggagaaggggtggtt	TD 70-60	304	63, 64
13	ccgggcacgtcaagctgtct	tcatgtcatgcactttggagg	TD 70-60	264	62, 63
14	ccccagccctaccaccc	gcaggagcttcacgttcaca	TD 70-60	248	61, 62
15A	ttcccaccactgactctct	actcttggcctcccctct	TD 65-55	328	59, 62
15B	gggatggggctggggga	ctgtgctacttctggccat	TD 70-60	338	63, 64
15C	tactggcatggtggttggg	gggaaaatggtgagactgtc	TD 70-60	359	62, 64
15D	aggagactgtggagactg	tgtatgcgatgtaaatgcc	TD 70-60	326	62, 63
15E	ggggttcctctgggcatta	cttcgatggcatcttgacgc	TD 70-60	311	55, 56

The table shows the number of exons, primers sequences, annealing temperature (T_a), product size (bp) and dHPLC temperature (dHPLC T).

TD= Touchdown PCR.

Table 4: PCR conditions of *KCNE1* and *KCNE2* exons.

KCNE1 exons	Forward primer (5'→3')	Reverse primer (5'→3')	PCR T _a (°C)	Product size (bp)
3.1	ctgcagcagtggaaccttaatg	gttcgagtgctccagcttctg	58	253
3.2	gggcatcatgctgagctacat	ttagccagtggtgggttca	58	233
3.3	gttcagcaggtggcaacat	gccagatggtttcaacgaca	58	281
KCNE2 exons	Forward primer (5'→3')	Reverse primer (5'→3')	PCR T _a (°C)	Product size (bp)
1	gcatctccctcccacttta	ttagcttgggtgcctttctcc	51	495

The table shows the number of exons, primers sequences, annealing temperature (T_a) and product size (bp). All the amplicons were analyzed by automatic sequencing.

4.3 Mutation Screening: dHPLC and Sequencing Analysis

PCR products were analyzed by dHPLC to search for mutation and/or polymorphism in SCN5A, KCNH2 and KCNQ1 genes. The conditions of dHPLC analysis are listed in table 1, 2 and 3. Samples evaluated by dHPLC that showed abnormal elution profile were analyzed using automatic sequencing (ABI-PRISM 3730 DNA Sequencer, Applied Biosystem) at CEINGE facility. The KCNE1 and KCNE2 genes were analyzed only by automatic sequencing.

4.4 RNA Extraction

Total RNA was extracted both from whole peripheral blood and eukaryotic transfected cells using TriPure Isolation Reagent (Roche Diagnostic, Indianapolis, IN). Five volumes of 0.2% NaCl were added to whole blood to obtain blood cells lysis. Sample was centrifugated at 1300 rpm for 10 minutes at 4°C. This step was repeated 2 times. Afterward, 1 ml of TriPure Isolation Reagent were added to the pellet. Cells were then lysed by repetitive pipetting or homogenization. Chloroform (200 µl) was added and the homogenates sample was centrifugated at 13000 rpm for 5 min at 4°C to separate the solution in 3 phases. The upper colorless phase was saved and isopropanol (500 µl) was added to precipitate RNA. Sample was centrifugated at 1200 rpm for 10 min at 4°C. One milliliter of 75% Ethanol was used to wash the pellet and sample was centrifugated again. Supernatant was discarded and pellet was air-dried and then was resuspended in RNase-free water.

For adherent cells, 1 ml of TriPure was added directly to the cell culture dish and cells were scraped from the wall of dish. Cell lysate was saved and syringed. Afterward, the lysate was treated with chloroform. Next steps are the same of the RNA extraction from whole blood.

4.5 Reverse Transcriptase PCR

RNA extracted from blood or transfected cells was used to obtain cDNA by Reverse Transcriptase PCR (RT-PCR).

The reaction was performed using SuperScript VILO cDNA synthesis kit (Invitrogen, Carlsbad, CA). The following reagents were used in 20 µl reaction volume adding: 4 µl of 5X VILO Reaction Mix (containing random primer, MgCl₂ and dNTP), 2 µl of 10X SuperScript Enzyme Mix, 2 µg of RNA and water.

The reaction was incubated at:

- 25°C for 10 minutes;
- 42°C for 60 minutes;
- 85°C for 5 minutes.

To check the success of cDNA synthesis, porphobilinogen gene, as control, was amplified by PCR.

The cDNA regions of hH1 spanning from exons 21-25 and exons 22-24 were amplified by PCR using Expand Taq High Fidelity PCR System (Roche Diagnostic, Indianapolis, IN). The primers used for PCR are listed in table 5 and PCR conditions are shown in table 6.

Table 5: Primers used to perform PCR of hH1 cDNA regions.

hH1 cDNA Region	Forward primer (5'-3')	Reverse primer (5'-3')
Exon 22-24	GTCACGATTTGAGGGCATG	AATGTCCATCCAGCCTTTAA
Exon 21-25	TTCTGCTTGAGTATGCCGACA	GTATTCCCCTGAGGCTGCT

Table 6: Cycling parameters applied to perform Expand Taq High Fidelity PCR.

hH1 cDNA REGION	SEGMENT	CYCLES	TEMPERATURE	TIME
Exon 21-25	1	1	94°C	5 min
			94°C	30 sec
	2	10	56°C	30 sec
			72°C	45 sec
			94°C	30 sec
			55°C	30 sec
			72°C	45 sec
			72°C	45 sec
	3	25	94°C	30 sec
			55°C	30 sec
72°C			45 sec	
72°C			45 sec	
4	1	72°C	7 min	
		72°C	7 min	
Exon 22-24	1	1	94°C	5 min
			94°C	15 sec
	2	10	58°C	30 sec
			72°C	45 sec
			94°C	15 sec
			57°C	30 sec
	3	25	94°C	15 sec
			57°C	30 sec
			72°C	45 sec (+5 sec each cycle)
	4	1	72°C	7 min
72°C			7 min	

4.6 Minigene: Construction and Expression

The genomic region of SCN5A spanning from exon 21 to exon 24 (minigene) was amplified by Expand Long Template PCR System (Roche Diagnostic, Indianapolis, IN). The following primers were used: forward primer: accatggccttcgaggacatctacct and reverse primer: aatgtccatccagccttta. The PCR conditions are showed in table 7.

The Kozak consensus sequence with an ATG initiation codon (accatgg) for proper initiation of translation was inserted in the forward primer. The reverse primer was designed in such a way to be in frame with the vector to permit the transcription of V5 epitope and polyhistidine tag. The PCR product was cloned in pcDNA3.1/V5-His/TOPO TA vector (Invitrogen, Carlsbad, CA) (fig. 12): the following reagents were used in 20 μ l reaction volume: 2 μ l of fresh PCR product, 1 μ l of Salt solution (1.2 M NaCl; 0.06 M MgCl₂), 1 μ l of vector. The reaction was incubated at room temperature for 5 minutes. The final construct were transformed in One Shot TOP10 chemically competent cells (Invitrogen, Carlsbad, CA) according to manufacturer's instructions. The final construct was sequenced to verify the proper insertion of the fragment into the vector.

Afterward, 1 μ g of plasmid was transfected in HEK 293 cells using Lipofectamine 2000 (Invitrogen, Carlsbad, CA). The mRNA was extracted from cells, as described previously, 48 hours after transfection.

Table 7: Expand Long Template PCR conditions used to amplify the spanning region from exon 21 to exon 24 of SCN5A gene.

SEGMENT	CYCLES	TEMPERATURE	TIME
1	1	94°C	5 min
2	10	94°C	30 sec
		59°C	1 min
		68°C	8 min
3	25	94°C	30 sec
		57°C	1 min
		68°C	8 min (+20 sec each cycle)
4	1	68°C	10 min

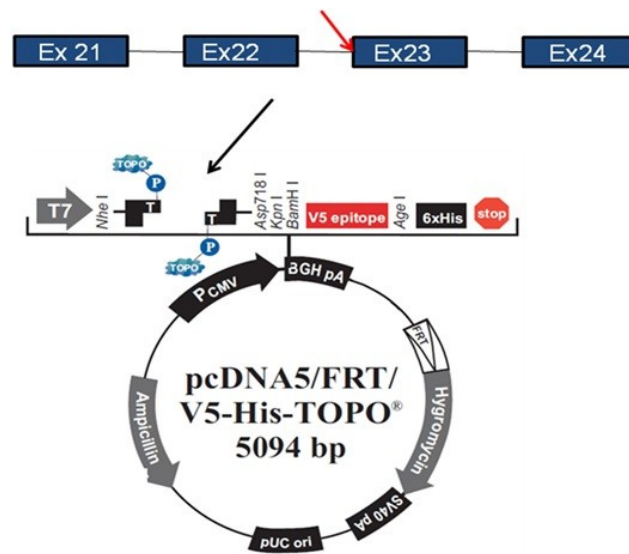


Figure 12: Schematic representation of *SCN5A* minigene (on the top) and vector. The red arrow shows the position of mutation; the black arrow shows the position where the minigene was inserted.

4.7 Site-directed Mutagenesis

The mutants, corresponding to unknown mutation found by genetic analysis, were generated to perform the in vitro expression studies.

The human cardiac sodium channels cDNA (hH1) was cloned in pRcCMV (Invitrogen, Carlsbad, CA) whereas human cardiac potassium channel cDNAs (KCNQ1 and HERG) were cloned in pIRES2EGFP (Clontech, Mountain View, CA). All plasmids were kindly provided by Dr. Alfred L. George. The mutants, corresponding to unknown mutations, were generated by QuickChange site-directed mutagenesis kit (Stratagene, La Jolla, CA). The primers were designed according to manufacturer's instruction (tab. 8). The mutagenesis reaction was performed in 50 mL final volume containing 1X reaction buffer (10 mM KCl, 10 mM (NH₄)₂SO₄, 20 mM Tris-HCl pH 8.8, 2 mM MgSO₄, 0.1% Triton X100, 0.1 µg/µl BSA), 0.3 mM dNTP, 125 ng of each primer, 2.5 U Pfu Turbo DNA polymerase and 50 µg of WT plasmid. The cycling parameters were listed in table 9. The mutagenesis products were treated with DpnI enzyme that is specific for methylated and hemimethylated DNA and is used to digest the parental DNA template and to select for mutation-containing synthesized DNA. Afterwards, all constructs were transformed in JM109 competent cells (Stratagene, La Jolla, CA) and purified using PureLink HiPure plasmid maxiprep kit (Invitrogen, Carlsbad, CA)

according with instructions. Final constructs were sequenced to verify creation of mutation and exclusion of polymerase errors.

Table 8: List of primer used to generate mutants by site-direct mutagenesis.

GENE	PRIMER	SEQUENCE (5' - 3')
SCN5A	T1808C Fw	gcaatgggggtgtctcat <u>C</u> actgggggcaggcgaccc
	T1808C Rev	gggtcgctgccccagt <u>G</u> atgagaccacccattgc
	G2284A Fw	cttcacagggattttcaca <u>A</u> cagagatgacctcaagatcattgc
	G2284A Rev	gcaatgatcttgaaggtcatctgt <u>T</u> tgaaaaatccctgtgaag
	G3964T Fw	gatttgaggcatgagg <u>T</u> tgggtggaatgccctggtggcg
	G3964T Rev	gcgccaccagggtaccaccca <u>A</u> cctcatgccctcaaac
	C3989A Fw	caatgccctggtggcg <u>A</u> catcccgtccatcatgaac
	C3989A Rev	gttcatgatggacgggatg <u>T</u> cgcccaccaggcattg
	4416-4418 AACdel Fw	tggtgcatcattgac-ttcaaccaacagaag
	4416-4418 AACdel Rev	cttctgttggttgaa-gtcaatgatgacacca
KCNH2	G323A Fw	gagctgcttctatAtctggtggtgtgtaccctgaagaacg
	G323A Rv	cgttcttcacgggtaccacatccaccagaTataggaagcagctc
	1450_1467agccacccggccgc del Fw	ccaacgaggaggtggtc-gccgtccactactcaagg
	1450_1467agccacccggccgc del Rv	ccttgaagttagtgacggc-gaccacctcctcgttgg
KCNQ1	824_826TCTdel Fw	gtacatcggcttctagcctcatct-cctcgtactttgtgta
	824_826TCTdel Rev	tacacaaagtacgagg-agatgaggcctaggaagccgatgtac
	G1748A Fw	ccctcactgttcatctcgggtcagaaaaagagcaaggatc <u>A</u> cggcagc
	G1748A Rev	aacacgatc
	G1748A Rev	gatcgtgttctgcccTgatccttctctttctgagaccgagatgaaca gtgagg

The uppercase and underlined base represents the nucleotide substitution, the bold dash shows the position of deletion.

Table 9: Cycling parameters applied for the mutagenesis reaction.

SEGMENT	CYCLES	TEMPERATURE	TIME
1	1	95°C	5 min
2	18-22	95°C	30 sec
		55 °C	30 sec
		68°C	2 min/Kb of plasmid length
3	1	68°C	10 min

4.8 Cell Cultures and Heterologous Expression

Cells tsA201 (or HEK293), for SCN5A experiments, were grown in Dulbecco's modified eagle medium supplemented with 10% Fetal Bovine Serum (FBS), 2 mM L-glutamine and 1% penicillin/streptomycin in a humidified, 5% CO₂ atmosphere at 37°C. Cells were transiently transfected with pRC-CMV-hH1 WT or hH1-mutants using FuGENE6 (Roche Diagnostic, Indianapolis, IN) or Lipofectamine 2000 (Invitrogen, Carlsbad, CA). In combination with hH1-WT or mutants was transfected a bicistronic plasmid (pGFP-IRES-hβ1), kindly provided by Dr. Alfred L. George, encoding enhanced green fluorescent protein and the human β1 subunit (hβ1) under the control of the cytomegalovirus immediate early promoter. Transfection was performed with 1 μg of sodium channel α subunit-encoding plasmid (pRC-CMV-hH1) and 0,6 μg of β1 subunit-encoding plasmid (pGFP-IRES-hβ1).

On the other hand, CHO-K1 cells were used for KCNH2 and KCNQ1 experiments. Cells were grown in F-12 nutrient mixture medium supplemented with 10% FBS, 2 mM L-glutamine, 1% Penicillin/Streptomycin and in a humidified, 5% CO₂ atmosphere at 37°C. For KCNH2 experiments, cells were transiently transfected using FuGene 6 with 1,5 μg of KCNH2-WT or KCNH2 mutants, whereas, for co-expression experiments, cells were transfected with 1,5 μg of both KCNH2-WT and mutant or KCNH2-WT and pDsRed empty vector.

For KCNQ1 experiments, CHO cells were transiently transfected with 1 μg of KCNQ1-WT or KCNQ1-mutants. Also, KCNQ1-WT and mutants were expressed in presence of 1 μg of KCNE1 (assembled in pIRES-DsRed vector) to study I_{Ks} channel complex.

4.9 Immunofluorescence

Cells were seeded onto glass coverslips 24 hours before transfection. Forty-eight hours after transfection cells were fixed with 4% paraformaldehyde and permeabilized in 0.2% TRITON X-100 (Roche, Diagnostic, Indianapolis, IN). Afterward, cells were incubated in blocking buffer (10% FBS and 2% Bovine Serum Albumine).

After blocking, cells were incubated with rabbit anti-SCN5A IgG (Chemicon, Catecula, CA) and then with rhodamine-conjugated goat anti-rabbit secondary antibody (Chemicon, Catecula, CA). Images were taken at 40X magnification on an LSM microscope (Carl Zeiss MicroImaging, Thornwood, NY).

4.10 Electrophysiology

Sodium and potassium currents were recorded at room temperature using patch-clamp technique in whole-cell configuration. Transfected cells were plated on glass coverslips approximately 2-3 hours before recording. Patch pipettes were pulled from borosilicate thin-wall glass (Warner Instrument, Hamden, CT) with a multistage P-97 Flaming-Brown micropipette puller (Sutter Instrument, San Rafael, CA) and fire-polished with a Micro Forge MF-830 (Narashige, Japan). Electrodes resistance ranged from 1.2 to 1.7 M Ω for sodium channel studies and from 2,5 to 4 M Ω for KCNH2 and KCNQ1 experiments.

For SCN5A experiments, the bath solution contained 140 mM NaCl, 10 mM HEPES, 4 mM KCl, 1 mM MgCl₂, 1.8 mM CaCl₂, 10 mM glucose, pH 7.35 (adjusted with NaOH). The pipette solution (intracellular solution) contained 10 mM NaF, 110 mM CsF, 20 mM CsCl, 2 mM EGTA, 10 mM HEPES, pH 7.35 (adjusted with CsOH). The bath and pipette solutions osmolarity was adjusted with sucrose to 310 and 300 milliosmoles respectively. Junction potential and pipette capacitance were corrected, and series resistance was 90% compensated to minimize voltage errors. Sodium currents were filtered at 5 KHz and leak current was subtracted using a P/4 protocol. Whole cell capacitance was determined by integrating the capacitive transient elicited by a 10 mV voltage step from -120 (holding potential) to -130 mV with 5 KHz filtering.

For KCNH2, the bath solution consisted of 145 mM NaCl, 4 mM KCl, 1 mM MgCl₂, 1,8 mM CaCl₂, 10 mM HEPES and 10 mM glucose, pH 7,35. The osmolarity was adjusted to 275 milliosmoles. The pipette solution contained 110 mM KCl, 2 mM MgCl₂, 10 mM EDTA, 10 mM HEPES and 5 mM K₂-ATP, pH 7,2. The osmolarity was adjusted to 255 milliosmoles.

For KCNQ1 and I_{Ks} experiments, the bath solution contained 132 mM NaCl, 4,8 mM KCl, 1,2 mM MgCl₂, 2 mM CaCl₂, 10 mM HEPES, 5 mM glucose, pH 7,4. The pipette solution contained 110 mM K-aspartate, 1 mM CaCl₂, 1 mM MgCl₂, 11 mM EGTA, 10 mM HEPES, 5 mM K₂-ATP, pH 7,3. The bath and pipette solutions osmolarity was adjusted to 280 and 260 missiosmoles respectively. Whole-cell currents were filtered at 5 KHz and leak current was not subtracted. Whole cell capacitance was determined by integrating the capacitive transient elicited by a 5 mV voltage step from -80 (holding potential) to -75 mV with 5 KHz filtering.

Before the experiments, the pipette solutions were diluted 7% (for KCNQ1) or 10% (for KCNH2) with sterile water to avoid activation of swelling-activated currents. Junction potential was corrected and series resistance was 90% compensated to minimize voltage errors. As reference electrode, a 2% agar bridge with composition similar to bath solution was used.

Only cells expressing fluorescence were selected for patch clamp recording. Cells showing very large or very slow whole-cell currents were not selected for data analysis (both sodium and potassium). Data acquisition was carried out

with Axopatch 200 amplifier and pClamp 10.0 software (Axon Instruments, Sunnyvale, CA).

4.11 Data Analysis

All data were analyzed using Clampfit 10 (Axon Instruments, Sunnyvale, CA) and SigmaPlot 11 (SPSS Science, Chicago, IL).

Sodium channels activation curve was fit with *Boltzmann* equation $I = (V - V_{rev}) \times G_{max} \times (1 + e^{[V - V_{1/2}]/k})^{-1}$ to determine the membrane potential at half-maximal activation ($V_{1/2}$) and slope factor (k). To determine the sodium channel inactivation parameters ($V_{1/2}$ and k) the current–voltage relationship was fit with Boltzmann equation $I/I_{max} = 1/(1 + e^{[V - V_{1/2}]/k})$.

Recovery from inactivation of sodium channel was evaluated by fitting data both with double-exponential equation $I/I_{max} = A_{fast}(1 - e^{-t/\tau_{fast}}) + A_{slow}(1 - e^{-t/\tau_{slow}})$ and single-exponential equation $I/I_{max} = A_{fast}(1 - e^{-t/\tau_{fast}})$, where A and τ are amplitudes and time constants respectively.

The level of tetrodotoxin (TTX) sensitive persistent sodium current was analyzed with a 200-ms depolarization protocol to -30 mV. The presence of inward persistent sodium current was determined as the average current recorded between 195 and 200 ms and expressed as percentage of peak current after digital subtraction of currents recorded in absence and in presence of 30 μ M TTX.

The voltage dependence of activation in KCNH2-WT+KCNH2 C108Y and KCNH2-WT + empty vector was fit with Boltzmann equation $I = (V - V_{rev}) \times G_{max} \times (1 + e^{[V - V_{1/2}]/k})^{-1}$.

In KCNQ1 experiments the voltage-dependence of activation was obtained by fitting data with the Boltzmann function: $I/I_{max} = 1/(1 + e^{[V - V_{1/2}]/k})$. The time course of deactivation, was calculated by fitting tail currents with a single exponential function $I = A \times \exp(-t/\tau) + I_0$.

All data (SCN5A, KCNH2 and KCNQ1) were presented as mean \pm SEM and statistical comparisons were estimated with Student's t test. Statistical significance was assumed for $P < 0.05$.

Chapter 5

RESULTS

5.1 Genetic Analysis

We carried out the genetic analysis in 49 patients affected by LQTS and 54 patients showing BrS phenotype. In the first step, the dHPLC analysis of SCN5A, KCNH2, KCNQ1, KCNE1, KCNE2 genes revealed several divergent elution profiles. Afterward, the automatic sequencing confirmed the presence of sequence variation (mutation or polymorphism) in PCR fragments showing abnormal chromatographic profile.

We identified 6 novel mutations in SCN5A gene: c.T1808C (p.L603S), c.G3964T (p.V1322L), c.C3989A (p.A1330D) and c.4416-4418 AAC del (p.ΔN1472) related to LQTS; c.G839A (p.C280T) c.G2284A (p.A762T) linked to BrS.

The location of mutation is showed in figure 13.

We also found:

- 3 novel mutations in KCNH2 gene: c. G323A (p.C108Y), c.1450-1467del (p.S484-I489del) and c.T245C (p.I83T);
- 1 novel mutation in KCNQ1 gene: c.824-826TCTdel (p.F275del) and
- 2 novel mutations in KCNE1 gene: c.C29T (p.T10M), c.G238A (p.V80I).

These mutations were linked to LQTS.

The location of mutations was showed in figure 14, 15 and 16. All the mutations found in our laboratory were listed in table 9 and 10.

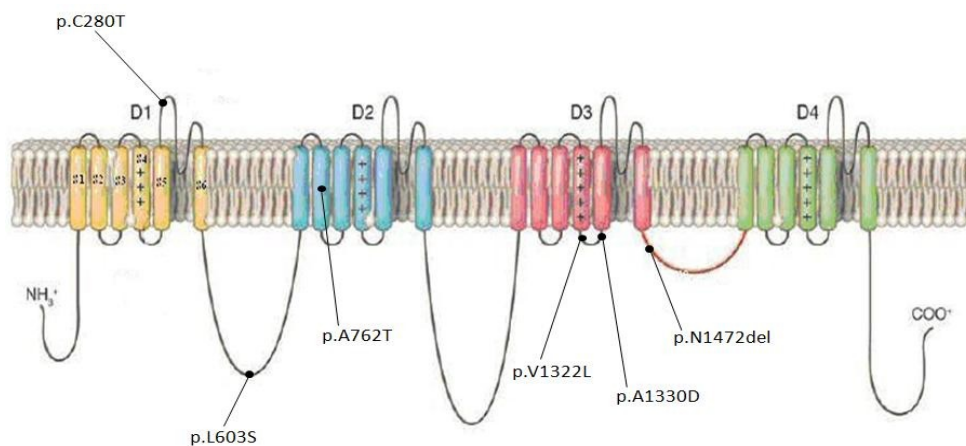


Figure 13: Location of novel mutations found in cardiac sodium channel α -subunit (hH1).

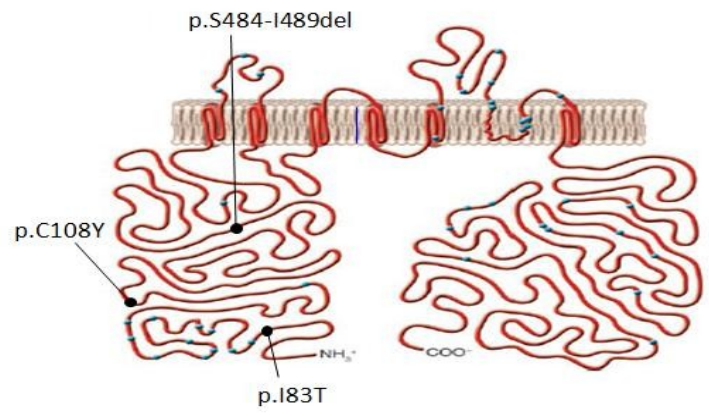


Figure 14: Location of novel mutations found in rapid rectifier potassium channel α -subunit (HERG).

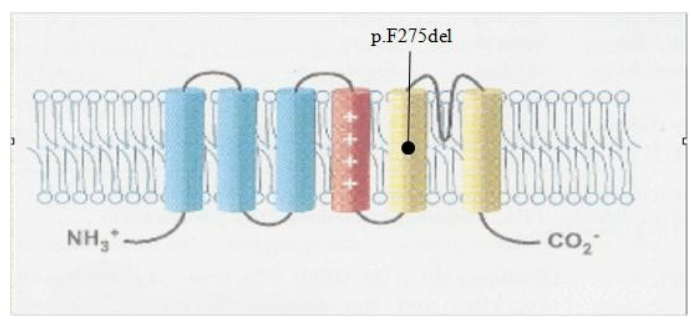


Figure 15: Location of novel mutations found in slow rectifier potassium channel α -subunit (KCNQ1).

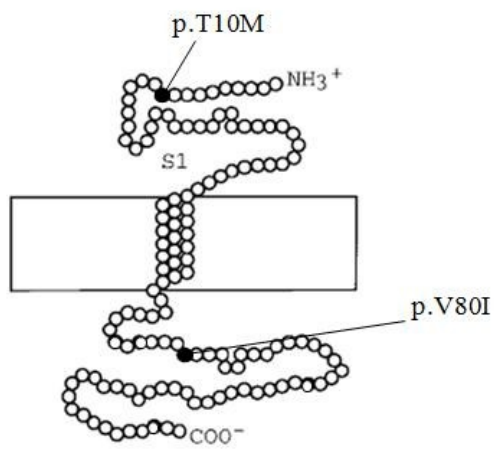


Figure 16: Location of novel mutations found in Mink1 β -subunit.

Table 9: Complete list of mutations (unknown and already described) found in SCN5A, KCNH2, KCNQ1, KCNE1 and KCNE2 genes in patients affected by long QT syndrome.

GENE	MUTATION	REFERENCE
SCN5A	c. T1808C (p.L603S)	UNKNOWN
	c.G3578A (p.R1193Q)	DESCRIBED
	c.G3964T (p.V1322L)	UNKNOWN
	c. C3989A (p.A1330D)	UNKNOWN
	c.4416-4418 AAC del (p.ΔN1472)	UNKNOWN
	c.G5350A (p.E1784K)	DESCRIBED
KCNH2	c.T245C (p.I82T)	UNKNOWN
	c. G323A (p.C108Y)	UNKNOWN
	c.1450-1467del (p. ΔS484-I489)	UNKNOWN
	c.C1682T(p.A561V)	DESCRIBED
	c.C1841T (p.A614V)	DESCRIBED
	c.C2230T (p.R744X)	DESCRIBED
	c.T2414C (p.F805S)	DESCRIBED
KCNQ1	c.524_534delTCTGGTCCGCC (p.R174fs105X)	DESCRIBED
	c.C691T (R231C)	DESCRIBED
	c.824-826TCTdel (p. ΔF275)	UNKNOWN
	c.A842G (p. Y281C)	DESCRIBED
	c.T910C (p.W304R)	DESCRIBED
	c.G1032A (p.A344A)	DESCRIBED
	c.G1573A (A525T)	DESCRIBED
	c. G1748A (p.R583H)	DESCRIBED
KCNE1	c.C29T (p.T10M)	UNKNOWN
	c.G238A (p.V80I)	UNKNOWN
	c.G253A (p.D85N)	DESCRIBED

Table 10: Complete list of mutations (unknown and already described) found in SCN5A gene in patients affected by Brugada syndrome.

GENE	MUTATION	REFERENCE
SCN5A	c.393-5C>A	DESCRIBED
	c.G481A (p.E161K)	DESCRIBED
	c.C647T (p.S216L)	DESCRIBED
	c.C655A (p.R219S)	UNKNOWN
	c.G839A (p.C280T)	UNKNOWN
	c.C1099T (p.R367C)	DESCRIBED
	c.G2284A (p.A762T)	UNKNOWN
	c.C3308CA (p.S1103Y)	DESCRIBED
	c.C3946T (p.R1316X)	DESCRIBED
	c.C4501G (p.L1501V)	DESCRIBED
	c.C4867T (p.R1623X)	DESCRIBED
	c.5420dupA (p.F1808VsfX3)	DESCRIBED
	c.G5458A (p.A1820T)	DESCRIBED
	c.G5796C (p.A1932A)	UNKNOWN

5.2 Splicing Analysis in One Patient Carrying the mutation SCN5A c.G3964T

The genetic analysis revealed the presence of a novel mutation, c.G3964T, in SCN5A gene that was located on the first base of exon 23. Thus, we studied the splicing mechanism in this patient.

Firstly, we performed *in silico* analysis using NetGene2 (<http://www.cbs.dtu.dk/services/NetGene2/>). This test showed that the confidence of acceptor splice site in SCN5A-c.G3964T is about 25% smaller compared to WT (WT: 0.95/1; c.G3964T: 0.74/1). Thus, we analyzed the mRNA (extracted from blood of patients carrying the mutation) amplifying the coding regions spanning from exon 21 to 25 and from exon 22 to 24. The PCR were then sequenced. This analysis showed that mutation c.G3964T induced alteration in splicing mechanism. The mRNA produced by the alternative splicing showed inclusion of 36 nucleotides between exon 22 and 23 (18

nucleotides from the beginning of exon 23 and 18 nucleotides from the end of exon 22) (fig. 17).

In addition, we generated the minigene containing genomic region from exon 21 to exon 24 of SCN5A gene. In this case, the mRNA produced from the minigene carrying c.G3964T mutation was similar to the WT. Supplementary experiments are underway.

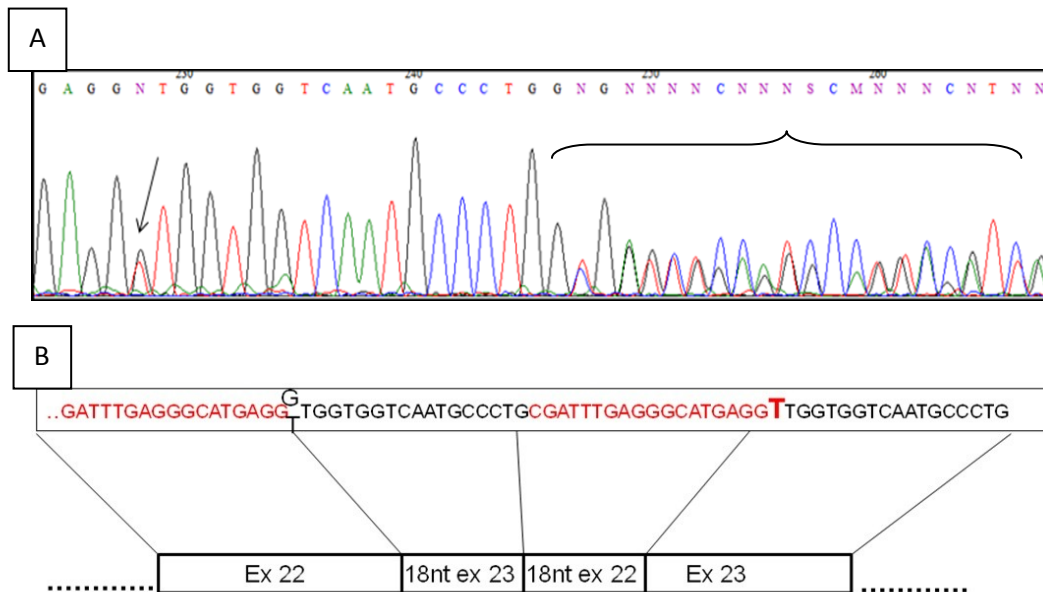


Figure 17: Analysis of mRNA in patient carrying SCN5A-c.G3964T mutations. (A) Electropherogram of cDNA region spanning from exon 22 to exon 24. The black arrow shows the mutation, the brace bracket shows alteration of sequence caused by insertion of 36 nucleotide. (B) Schematic representation of insertion between exon 22 and exon 23. The red sequence is related to exon 22, the black sequence is related to exon 23.

5.3 Immunofluorescence Studies

We transfected HEK293 with cardiac sodium channel α -subunit (emitting red signal) and human β 1 subunit (expressing green fluorescence) to evaluate the behavior and the cellular location of mutant protein.

Five unknown mutation found in SCN5A gene were analyzed by immunofluorescence technique: c.T1808C, c.G3964T, c.C3989A, c.4416_4418AACdel and c.G2284A. The latter is found in a patient affected by BrS whereas the first 4 mutations are related to LQTS patients. The immunofluorescence clearly shows that each mutant channel is located on the cell surface showing a correct cellular trafficking (figure 18).

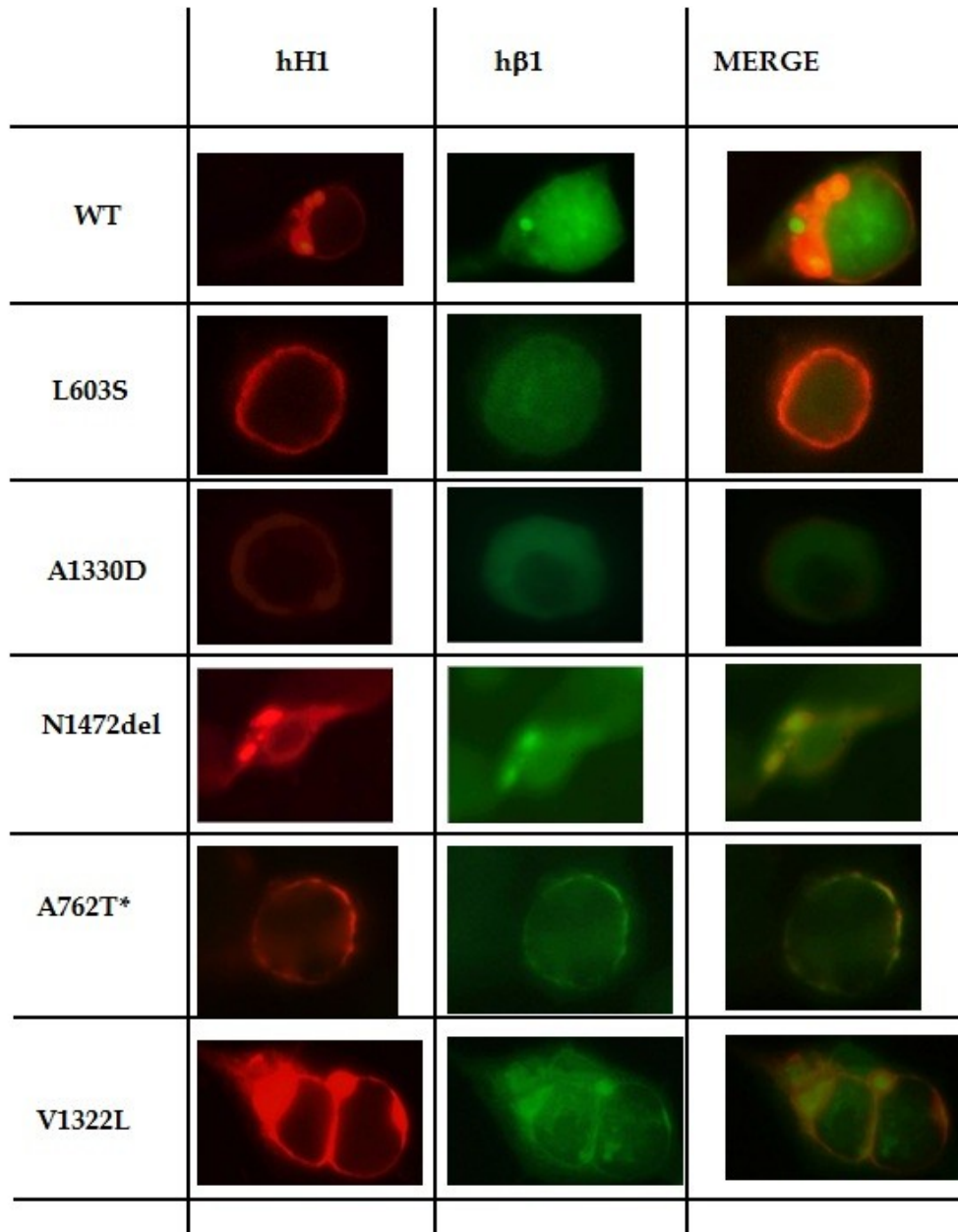


Figure 18: Immunofluorescent analysis of cardiac sodium channel mutant in HEK293 cells. Immunofluorescence was used to determine the expression and location of WT and mutant protein. Lane 1 (hH1) shows rhodamine staining of cardiac sodium channel α -subunit; Lane 2 (hβ1) shows FITC staining of ancillary β -subunit WT; Lane 3 (MERGE) shows merge of α and β subunit. The asterisk indicates the mutation associated to Brugada Syndrome, the remaining mutations are linked to long-QT syndrome.

5.4 Functional Characterization of Mutant Channels

In order to analyze the genotype-phenotype association and to shed light on the pathogenetic defects responsible for the LQTS cases we studied the biophysical features of sodium and potassium channels using the patch-clamp technique in whole-cell configuration.

5.4.1 Biophysical Properties of Mutant hH1-p.ΔN1472

Genetic analysis revealed that one patient carried a novel mutation (c.4416-4418delAAC) in cardiac sodium channel gene (SCN5A). We also analyzed and genotyped the family (fig. 19). The mutation caused the deletion of Asparagine 1472 in the intracellular DIII-DIV linker loop. Asparagine 1472 is highly conserved among homologous sequences in several species and along evolutionary scale. Functional analysis was performed in tsA201 cells transfected with hH1 WT or mutant, in combination with β -subunit.

The functional studies of p.ΔN1472 performed by whole-cell patch clamp revealed that mutant has the peak current density approximately 50% smaller compared to hH1-WT channel (p.ΔN1472 : 156.6 ± 21 pA/pF n=25; hH1-WT: 328 ± 56 pA/pF n=21; $P < 0.05$) and, also, the peak current of N1472del was shifted to more positive potential (fig 20A).

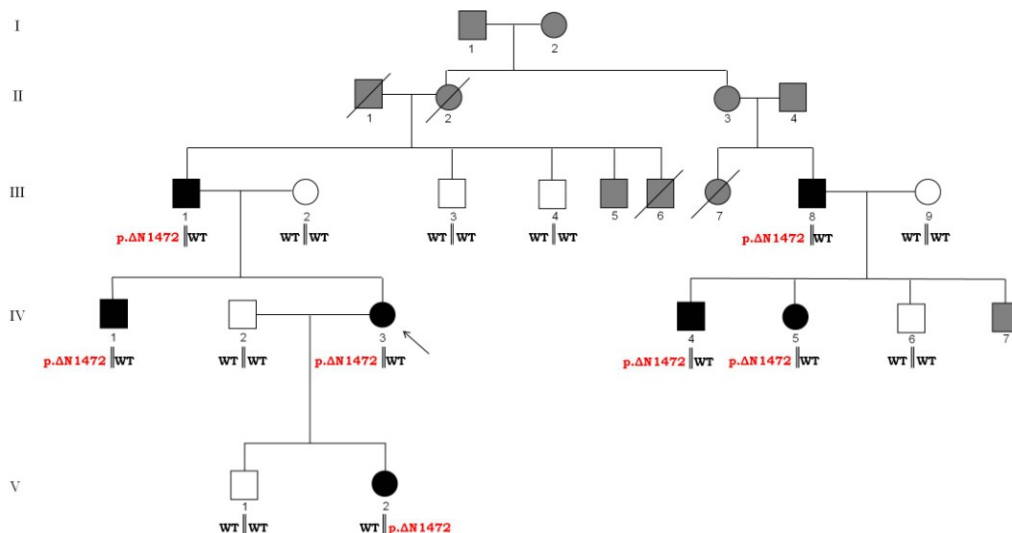


Figure 19: Pedigree of a family with LQTS3. All the patients carrying the mutation p.ΔN1472 show LQTS phenotype. The black, white and grey symbols represent affected patients, negative-phenotype and not analyzed subjects respectively. The arrow shows the proband.

First, we tested the voltage dependence of activation using a depolarizing protocol from -80 to +60 mV with 10 mV increments between each step. The mutant p. Δ N1472 showed depolarizing shift in voltage dependence of activation ($V_{1/2}$: p. Δ N1472, -28.86 ± 0.72 mV, $n=23$; hH1 WT, -44.41 ± 1.12 mV, $n=21$; $P < 0.001$) and increasing in slope factor (k : p. Δ N1472, 9.15 ± 0.17 , $n=23$; hH1-WT, 7.14 ± 0.29 , $n=21$; $P < 0.001$) (fig. 20B).

Moreover, we analyzed the voltage dependence of inactivation using the protocol shown as inset in figure 18 C. The mutant p. Δ N1472 exhibited a +12 mV depolarizing shift in steady-state of inactivation compared with WT ($V_{1/2}$: p. Δ N1472 -72.59 ± 0.53 , $n=21$; hH1-WT, -85.04 ± 1.83 , $n=24$; $P < 0.001$); instead the slope factor was similar ($k = -7.99 \pm 0.94$ and -6.78 ± 0.16 for WT and p. Δ N1472 respectively) (Fig. 20C). The shift in voltage dependence of activation and steady-state of inactivation implied that the window current, of p. Δ N1472 mutant was increased and shifted to more positive potential compared to hH1-WT (Fig. 20D). The window current is generated by overlap between activation and inactivation curve.

We also analyzed the TTX-sensitive persistent sodium current using a 200-ms depolarizing protocol at -30 mV from holding potential of -120 mV. The persistent current experiment revealed that p. Δ N1472 mutant had clearly increased levels of persistent sodium current compared to hH1-WT (p. Δ N1472: 2.64 ± 0.25 % $n=5$; hH1-WT: 0.08 ± 0.02 % $n=5$; $P < 0.001$) (fig. 21). Importantly, the increasing in persistent current is a typical feature of SCN5A mutations associated with LQTS type 3.

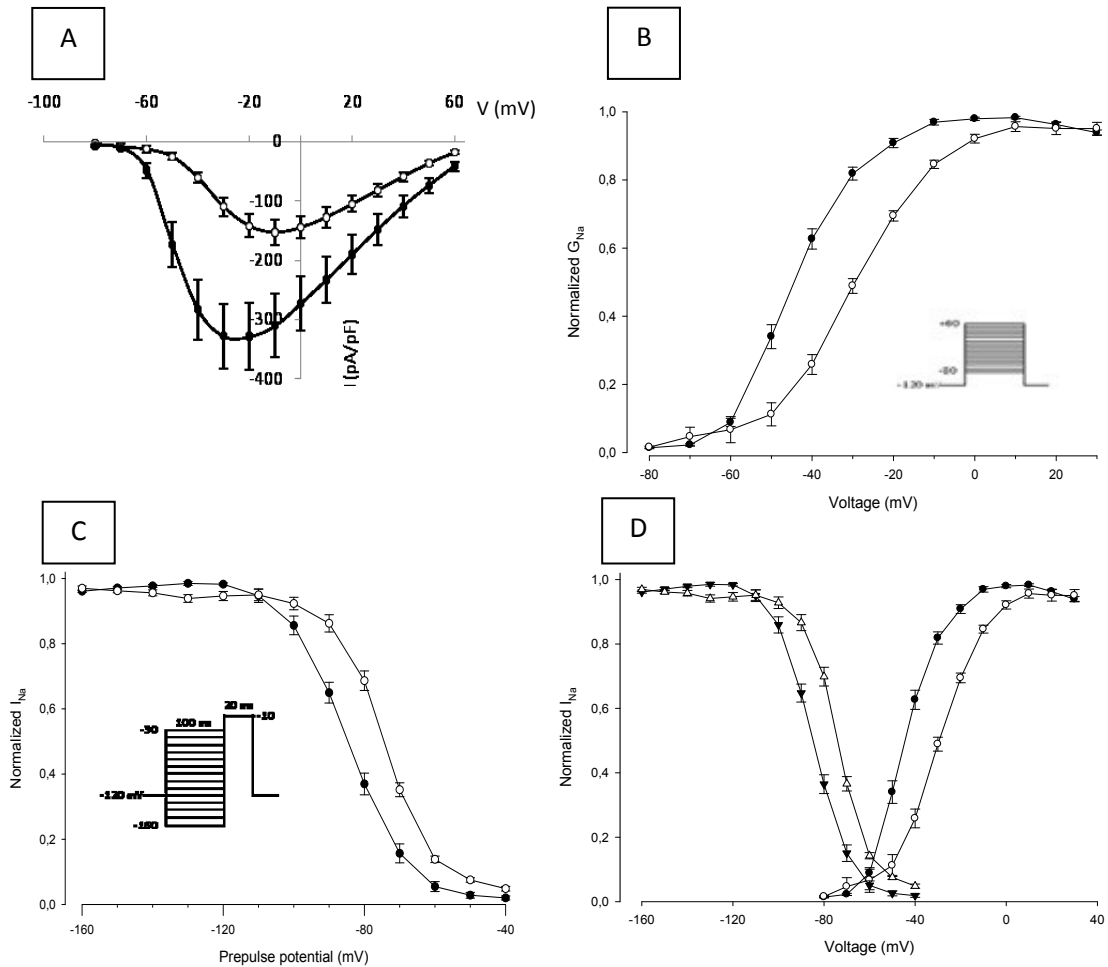


Figure 20: Biophysical properties of p.ΔN1472 and hH1-WT sodium channel. (A) Current-voltage relationship for hH1-WT (filled circles) and p.ΔN1472 (open circles). Currents were normalized from cell capacitance to give a measure of sodium current density. There were significant differences in current density between WT and mutant. (B) Voltage dependence of sodium channel activation. Currents were recorded using the pulse protocol shown as an inset. Current-voltage curve was fit with Boltzmann distribution. Potential at half-maximal activation ($V_{1/2}$) and slope factor (k) are provided in Table x. (C) Voltage dependence of steady-state inactivation. Currents were normalized to the peak current amplitude. Parameters ($V_{1/2}$ and k) are listed in table x. (D) Window currents: superimposition between voltage-dependence of activation and inactivation in hH1-WT (filled circle for activation and filled triangles for inactivation) and p.ΔN1472 (open circle for activation and open triangles for inactivation).

In addition, we analyzed the recovery from fast inactivation applying a double-pulse protocol showed as inset in figure 22.

As result, the recovery from fast inactivation in the WT channel was characterized by a single, fast time constant parameter (τ fast) whereas the p. Δ N1472 mutant channel by a fast and a slow time constant parameters (τ slow, τ fast). This effect causes a significantly delayed recovery from inactivation in the mutant channel. As shown in the figure 20 after 40 ms at the resting potential (-120 mV) the WT channel recovered almost completely (96%); by contrast, the current of the p. Δ N1472 mutant channel after 40 ms was about 70%, in fact the mutant needed almost 1000 ms to almost fully recover. Moreover, the figure showed that the p. Δ N1472 mutant channels do not fully inactivate after 100 ms inactivating pulse (-10mV). In fact, after 1 ms at the resting potential the mutant channels still display 20% current, whereas the WT channels are almost fully inactivated (about 0% current).

All biophysical parameters are listed in table 11.

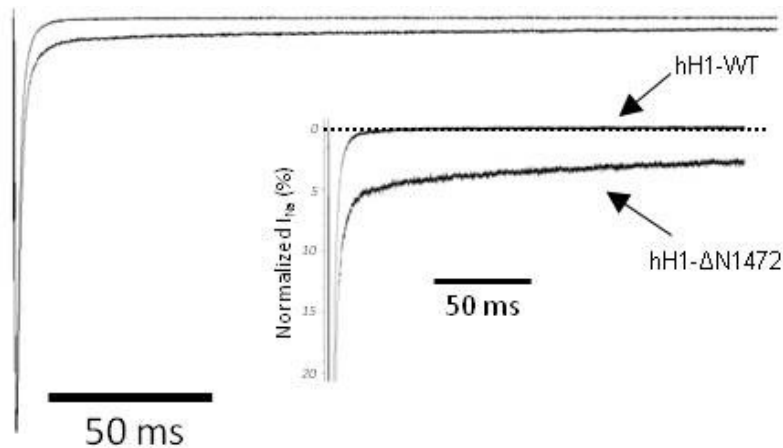


Figure 21: Increased TTX-sensitive persistent sodium current for p. Δ N1472. Zero current level is indicated by a dotted line. The inset shows an expanded y axes scale to emphasize the relative proportion of hH1-WT and p. Δ N1472 currents.

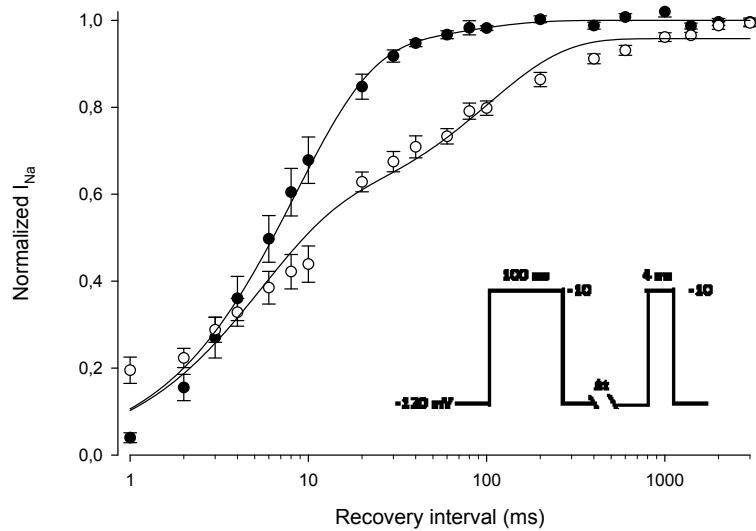


Figure 22: Biophysical properties of *p.ΔN1472* and *hH1-WT* sodium channel. Recovery from inactivation performed by double-pulse protocol shown in inset. Current-time curve was fit with double-exponential equation.

Table 11: Biophysical parameters of *hH1-WT* and *p.ΔN1472* mutant.

Parameters	<i>hH1-WT</i>	<i>N1472del</i>
Voltage dependence of activation		
$V_{1/2}$ (mV)	$-44,41 \pm 1,12$	$-28,86 \pm 0,72^*$
k (mV)	$7,14 \pm 0,29$	$9,15 \pm 0,17^*$
n	21	23
Steady-state of fast inactivation		
$V_{1/2}$ (mV)	$-84,99 \pm 2,19$	$-72,59 \pm 0,53^*$
k (mV)	$-8,16 \pm 1,13$	$-6,78 \pm 0,16$
n	21	21
Persistent I_{Na} (%)		
	$0,08 \pm 0,02$	$2,64 \pm 0,25^*$
n	5	5

* $P < 0.001$ (Comparison with *hH1-WT* using Student's *t*-test).

5.4.2 Electrophysiological analysis of digenic heterozygosity in KCNQ1 and KCNH2 genes

The screening for LQTS-causing mutations revealed two mutations in two genes: c.G1748A (p.R583H) in KCNQ1 and c.G323A (p.C108Y) in KCNH2. The presence of both mutations was found in two subjects (II-2 and II-3 in figure 23). This condition is known as digenic heterozygosity. Interestingly, the two subjects carrying both mutations showed severe long QT phenotype; in fact, the QT interval was more than 530 milliseconds. The HERG-p.C108Y mutation occurs in N-terminus of protein and modifies a highly conserved amino acid residue. The KCNQ1-p.R583H mutation is located in transmembrane segment S5; the specific amino acid is highly conserved among homologous sequences in several species and along evolutionary scale.

5.4.2.1 Biophysical Properties of the Mutant HERG-p.C108Y

KCNH2-p.C108Y mutant channel was investigated by analyzing the ionic currents from CHO-K1 cells transfected with KCNH2-WT or KCNH2-p.C108Y and from CHO-K1 cells co-transfected with KCNH2-WT and KCNH2-p.C108Y.

Data were recorded at test potentials ranging from - 80 to + 70 mV stepped in 10 mV increments from the holding potential of - 80 mV for 2000 ms, followed by repolarization to - 50 mV for 2000 ms.

As results, the biophysical studies showed that cells expressing KCNH2-p.C108Y in homozygous condition had no current. So, the p.C108Y mutant channel is a non-functional channel (fig. 24A).

On the other hand, in order to evaluate if this mutant channel could exert a dominant negative effect in heterozygous condition, as observed in our patients (fig. 23), we recorded whole-cell we analyzed CHO-K1 cells co-expressing KCNH2-WT and KCNH2-p.C108Y. The mutant channel, in combination with KCNH2-WT, showed significantly reduced activating and tail currents densities (Fig. 24B, C). In particular, activating current density was reduced by ~50% and tail current density by ~63%. In addition, we analyzed the voltage dependence of activation in KCNH2 WT+KCNH2-p.C108Y, which was significantly shifted to more negative potentials (fig. 24D). ($V_{1/2}$: KCNH2-WT + empty vector, 12.9 ± 2.4 mV, $n=6$; KCNH2-WT + KCNH2-p.C108Y, -7.0 ± 3.1 mV, $n=9$; $p < 0.05$) but there were no differences in the slope factor (k : KCNH2-WT + empty vector, 10.75 ± 0.69 mV, $n=6$; KCNH2-WT + KCNH2-p.C108Y, 12.92 ± 0.85 mV, $n=9$; $p > 0.05$)

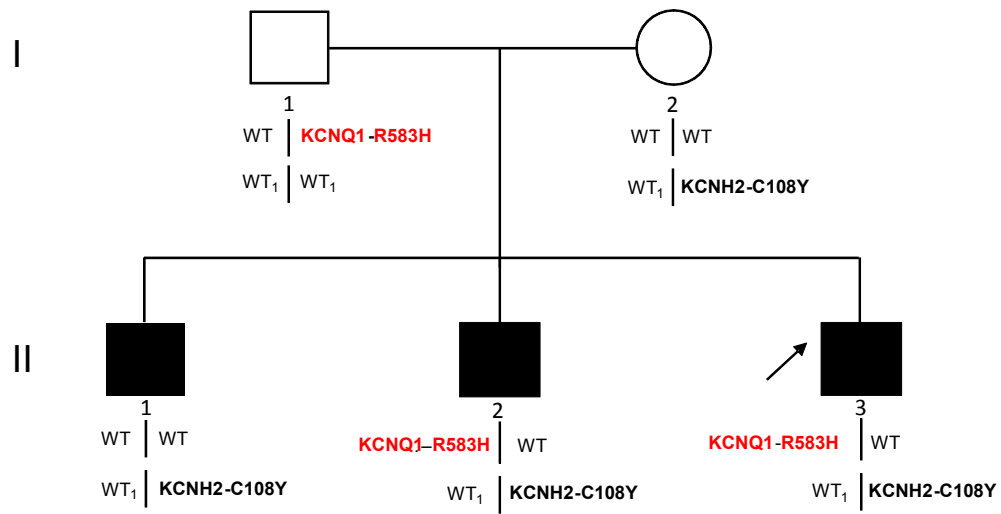


Figure 23: Segregation of *KCNQ1*-p.R583H (in bold red) and *KCNH2*-p.C108Y (in bold black) variants in the LQTS pedigree. Subjects carrying both the mutations show severe long QT phenotype. The solid symbols represent the individuals clinically affected. The arrow shows the proband.

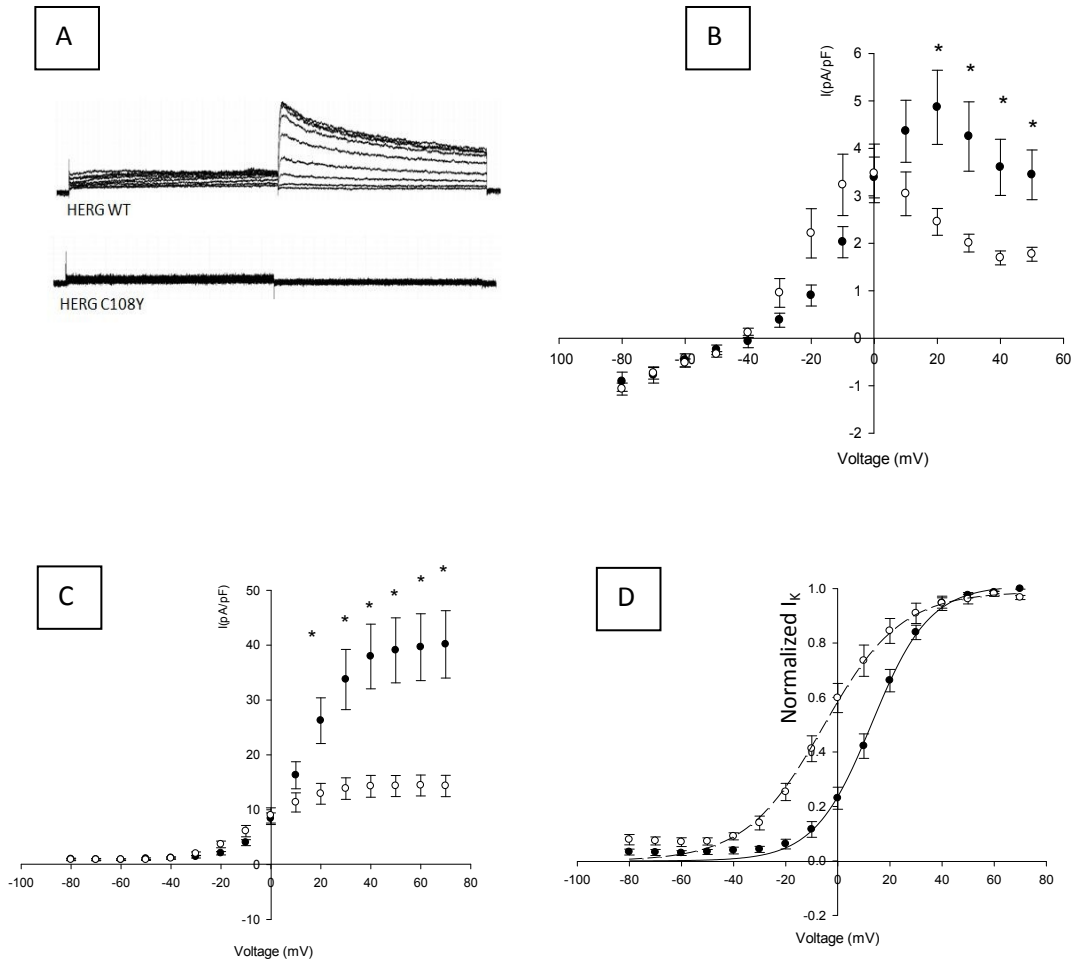


Figure 24: Functional characterization of KCNH2-p.C108Y variant. (A) representative traces illustrating K⁺ currents observed in CHO-K1 cells transiently transfected with KCNH2-WT or KCNH2-p.C108Y recorded with the protocol shown in inset (arrows indicate the time points at which currents were compared). (B) current-voltage relation for K⁺ current densities from CHO-K1 cells transiently transfected with KCNH2-WT + empty vector (solid circles) or KCNH2-p.C108Y + KCNH2-WT (open circles). (C) current-voltage relation for amplitude of peak tail current densities after repolarization to -50 mV for KCNH2-WT + empty vector (solid circles) and KCNH2-p.C108Y + KCNH2-WT (open circles). (D) normalized current-voltage relation for peak tail current densities for KCNH2-WT + empty vector (solid circles) and KCNH2-p.C108Y + KCNH2-WT (open circles, n = 9). Asterisk indicates significant differences between KCNH2-WT + empty vector and KCNH2-p.C108Y + KCNH2-WT (p < 0.05).

5.4.2.2 Biophysical Properties of the Mutant KCNQ1-p.R583H

In order to analyze KCNQ1 mutant properties, we transfected CHO-K1 cells with KCNQ1-p.R583H channels. The mutant channel showed no significant differences in activating and tail current values (fig. 25B, C). On the contrary, significant differences were observed in the activating processes and in tail current decays (Fig. 25A, 26). In particular, the KCNQ1-p.R583H mutant channels seem to undergo an inactivation process during the activation step which is not found in KCNQ1-WT channels. Furthermore, the time course of deactivation resulted to be altered in KCNQ1-p.R583H mutant channels compared to KCNQ1-WT channels (fig. 26). The fitting of tail currents by single exponential equation revealed that the time constants of deactivation are significantly faster in KCNQ1-p.R583H mutant channels (fig. 27). Moreover, we observed statistically significant positive shift in voltage dependence of activation ($V_{1/2}$: KCNQ1-WT, -22.3 ± 0.97 mV, $n=18$; KCNQ1-p.R583H, -16.7 ± 1.22 mV, $n=12$, $p < 0.05$) without significant alteration in the slope factor (k : KCNQ1-WT, 2.96 ± 0.59 mV, $n=18$; KCNQ1-p.R583H, 4.59 ± 1.15 mV, $n=12$, $p > 0.05$) (fig. 25D).

In addition, we characterized the functional defects carried by the KCNQ1-p.R583H mutant channels recording whole-cell currents in CHO-K1 cells co-expressing KCNQ1 and the accessory subunit KCNE1, to study the I_{Ks} complex.

As results, the currents recorded in KCNQ1-p.R583H + KCNE1 transfected cells didn't show any significant difference in activating currents, tail currents and voltage dependence of activation compared to KCNQ1-WT + KCNE1 transfected cells ($V_{1/2}$: KCNQ1-WT+KCNE1, -31.8 ± 6.0 mV, $n=7$; KCNQ1-p.R583H+KCNE1, 35.5 ± 5.9 mV, $n=8$, $p > 0.05$; k : KCNQ1-WT+KCNE1, 16.86 ± 0.93 mV, $n=7$; KCNQ1-p.R583H+KCNE1, 15.38 ± 1.15 mV, $n=8$, $p > 0.05$).

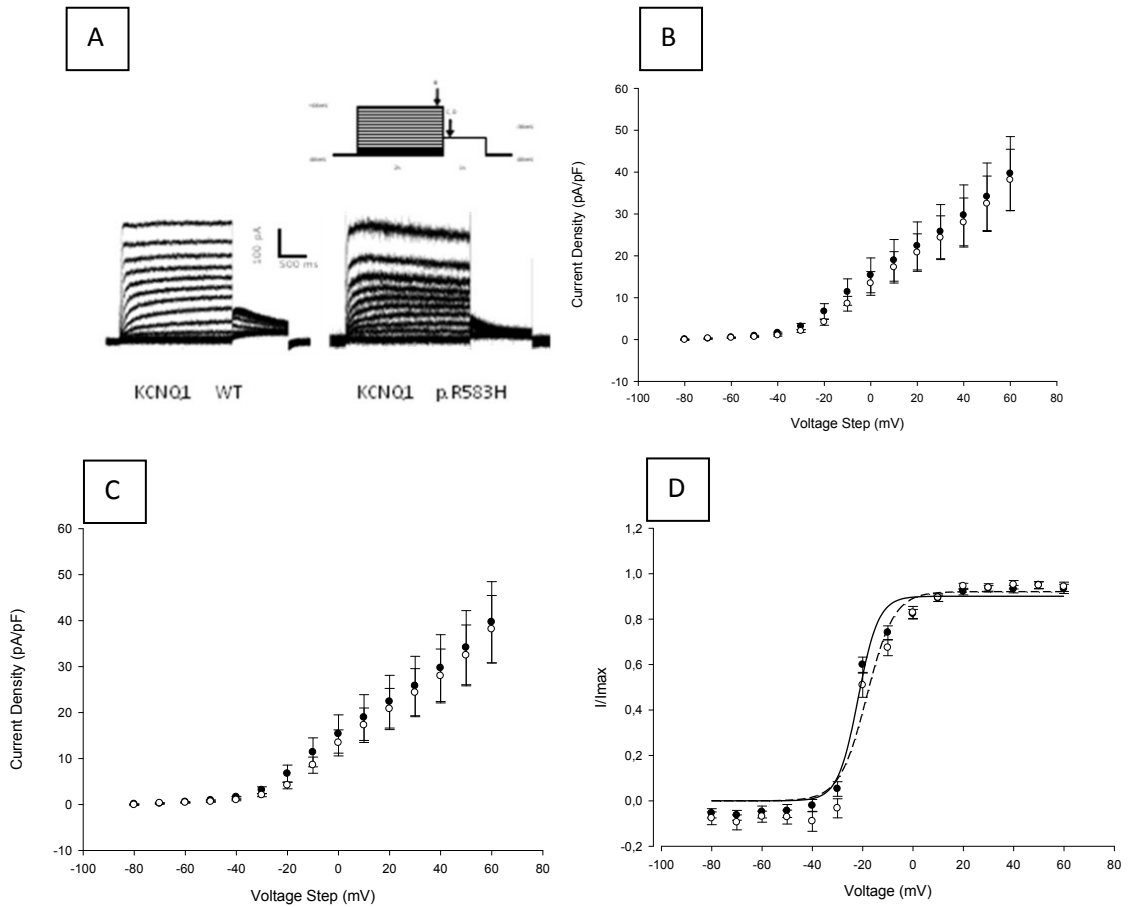


Figure 25: Function I characterization of $KCNQ1$ -p.R583H. (A) representative traces illustrating potassium currents observed in CHO-K1 cells transiently transfected with $KCNQ1$ -WT or $KCNQ1$ -p.R583H recorded using protocol shown as inset (arrows indicate the time points at which currents were compared). (B) current-voltage relation for potassium current densities from CHO-K1 cells transiently transfected with $KCNQ1$ -WT (solid circles) or $KCNQ1$ -p.R583H (open circles). (C) current-voltage relationship for amplitude of peak tail current densities after repolarization to -30 mV for $KCNQ1$ -WT (solid circles) or $KCNQ1$ -p.R583H (open circles). (D) normalized current-voltage relationship for peak tail current densities for $KCNQ1$ -WT (solid circles) and $KCNQ1$ -p.R583H (open circles). Data were recorded at test potentials ranging from -80 to +60 mV stepped in 10 mV increments from the holding potential of -80 mV for 2000 ms, followed by repolarization to -30 mV for 1000 ms. Data were fit with a Boltzmann distribution for $KCNQ1$ -WT (solid line) or $KCNQ1$ -p.R583H (dashed line).

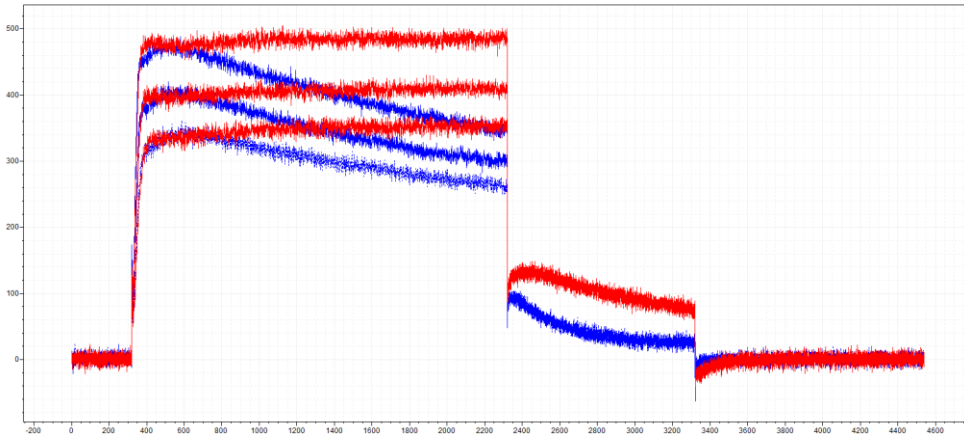


Figure 26: Functional characterization of *KCNQ1-p.R583H* mutant. Representative traces illustrating potassium currents observed in CHO-K1 cells transiently transfected with *KCNQ1-WT* (red trace) or *KCNQ1-p.R583H* (blue trace) recorded with the protocol showed as inset.

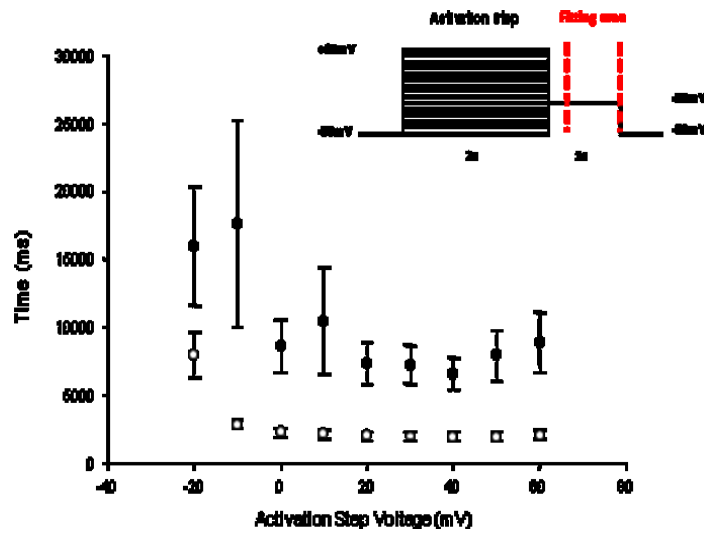


Figure 27: Time constants of tail current decay for *KCNQ1-WT* (solid circles) and *KCNQ1-p.R583H* (open circles). Data were obtained by fitting the tail current (area delimited by red dotted lines shown in inset) with a single exponential equation.

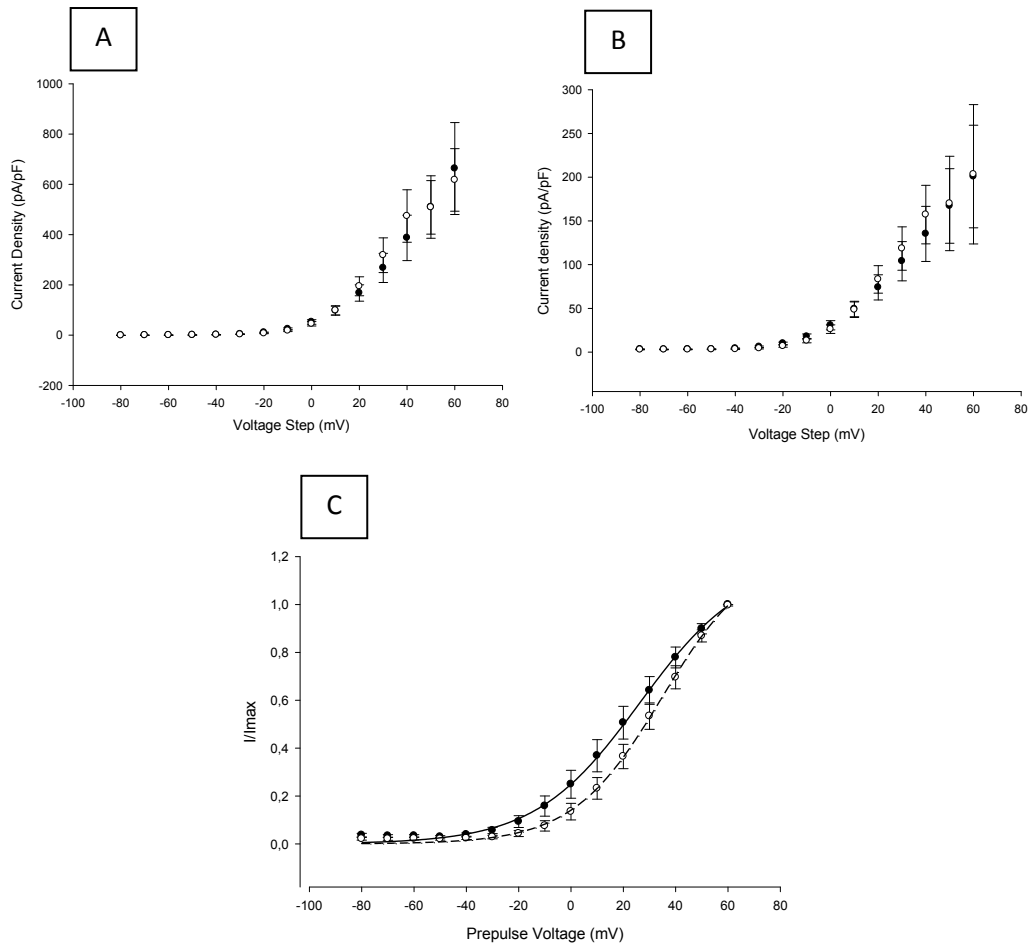


Figure 28: Functional characterization of IKs complex. (A) current-voltage relation for potassium current densities from CHO-K1 cells transiently transfected with KCNQ1-WT+KCNE1 WT (solid circles) or KCNQ1-p.R583H+KCNE1 WT (open circles). (B) current-voltage relationship for amplitude of peak tail current densities after repolarization to -30 mV for KCNQ1-WT+ KCNE1 WT (solid circles) or KCNQ1-p.R583H+KCNE1 WT (open circles). (C) normalized current-voltage relationship for peak tail current densities for KCNQ1-WT+ KCNE1 WT (solid circles) and KCNQ1-p.R583H+ KCNE1 WT (open circles). Data were recorded at test potentials ranging from -80 to $+60$ mV stepped in 10 mV increments from the holding potential of -80 mV for 2000 ms, followed by repolarization to -30 mV for 1000 ms. No difference were detected in KCNQ1-p.R583H+KCNE1 WT compared to KCNQ1-WT+KCNE1 WT.

Chapter 6

DISCUSSION

Long QT syndrome is a cardiac channelopathy characterized by prolonged QT intervals on the surface electrocardiogram, syncope and sudden cardiac death due to ventricular tachyarrhythmias, in particular torsade de pointes [Amin et al. 2009, Schwartz et al. 2001]. The disorder occurs in young subjects, especially in children and teenagers. Prolonged QT intervals reflect action potential duration in ventricular myocytes, and correspond to delayed ventricular repolarization [Amin et al. 2009]. The pathology is generally linked to mutations in SCN5A, KCNH2, KCNQ1, KCNE1 and KCNE2. These genes encode cardiac ion channels (SCN5A, KCNH2, KCNQ1) and ancillary β -subunits (KCNE1 and KCNE2).

6.1 Gain-of-function of Mutant hH1-p. Δ N1472

The voltage-gated cardiac sodium channel, SCN5A, conducts the inward sodium current (I_{Na}) that initiates the cardiac action potential. The SCN5A-mediated late sodium current also influences repolarization and refractoriness. Several diseases associated with ventricular conduction abnormalities have been associated with mutations in SCN5A, including LQTS and BrS. We identified 4 novel mutations in SCN5A related to LQTS. In particular, we functionally characterized the p. Δ N1472 mutation.

First, we found that persistent sodium current is clearly higher in the mutant than hH1-WT. Importantly, the increasing in persistent current is a hallmark of SCN5A mutations associated with LQTS type 3. This biophysical defect may explain the onset of LQTS.

In addition, mutant p. Δ N1472 shows a positive depolarizing shift in voltage-dependence of activation and a +12 mV depolarizing shift in the voltage dependence of inactivation. The positive shift in the activation and inactivation indicates that mutant channel opens and closes at a more positive voltage value compared to the WT; this means that the mutant channel opens and closes later than the WT. Furthermore, the mutant shows a significantly delayed recovery from inactivation. This alteration is not a typical characteristic of the long QT phenotype but it should cause other alteration not clinically detected or masked by LQTS. However, these biophysical defects alter the normal behavior of sodium channel: our data suggest that the mutant channel opens and closes later than WT channels and persistent sodium current is maintained. The increase in intake of sodium current causes the prolongation of action potential

plateau phase reflecting in the prolongation of the action potential duration. This biophysical behavior of the mutant is clearly the trigger for LQTS phenotype. In addition, the mutant shows additional functional properties, namely delayed recovery from inactivation and shift in the activation, that are uncommon in the LQTS, but are probably linked to other heart conduction defects.

6.2 Digenic Heterozygosity in KCNH2 and KCNQ1 Genes

The screening for LQTS-causing mutations in a family from South Italy revealed two mutations in two genes: c.G1748A (p.R583H) in KCNQ1 and c.G323A (p.C108Y) in KCNH2. These genes encode potassium channel α -subunits. Interestingly, subjects carrying both mutations showed a severe LQTS phenotype ($QTc \geq 530$ ms). This condition is known as digenic heterozygosity. We functionally characterized both mutations by whole-cell patch clamp. Interestingly, the KCNH2-p.C108Y mutant is a non-functional channel. Moreover, we analyzed the mutant in combination with WT (heterozygous condition). The results show that KCNH2-p.C108Y+KCNH2-WT had 50% reduced currents (activation and tail currents) suggesting that the KCNH2 mutation exerts a dominant negative effect when it is expressed in a heterozygous condition.

We also analyzed the functional properties of the KCNQ1-p.R583H mutant. This mutation has already been reported and associated to LQTS (Napolitano et al 2005). We found no significant differences in activating and tail current values between WT and mutant channels. On the contrary, we observed significant differences in the activating processes and in tail current decay, suggesting an inactivation process during the activation step.

Furthermore, the time course of deactivation resulted to be altered in KCNQ1-p.R583H mutant channels compared to KCNQ1-WT channels. In addition, the fitting of tail currents by single exponential equation revealed that the time constants of deactivation are significantly faster in KCNQ1-p.R583H mutant channels. The abnormal activation and deactivation kinetics observed in this mutant channel suggest that the mutation could alter the normal repolarizing process during the heart action potential. In contrast, when we co-expressed KCNQ1 (WT and mutant) with β -subunit (KCNE1) no differences were observed suggesting that LQTS phenotype cannot be led by this mutation.

The segregation of the two mutations in the affected subjects and the electrophysiological results indicate that the mutation KCNH2-p.C108Y is the cause for LQTS phenotype, whereas the mutation KCNQ1-p.R583H, alone, do not cause severe biophysical alterations to trigger for long QT syndrome. In fact, the subjects carrying both mutations show a very long QT interval ($QTc > 530$ ms) and, in this case, the clinical symptoms are not easily manageable by pharmacological therapy. Probably, the mutation KCNQ1-p.R583H variant could be a modifier of the HERG mutation.

In fact, as described by Brunner et al (2008), we presume that the KCNH2 and KCNQ1 mutants interact with the reciprocal WT α -subunits (KCNQ1-p.R583H/KCNH2-WT and KCNH2-p.C108Y/KCNQ1-WT) thereby causing an alteration in the WT channel function. These defects, in combination, may explain the severe LQT phenotype.

In conclusion, the proband's mother (I-2 in figure 23) shows just the mutation KCNH2-p.C108Y but does not manifest any symptoms. We assume that a genetic protective factor, not yet known, is present in the proband's mother.

ABBREVIATIONS

<i>A</i>	<i>Amperes</i>
<i>A_{fast}</i>	<i>Fast amplitude</i>
<i>AKAP9</i>	<i>A-kinase anchoring protein</i>
<i>ANK2</i>	<i>Ankyrin B</i>
<i>AP</i>	<i>Action potential</i>
<i>APD</i>	<i>Action potential duration</i>
<i>ARVC/D</i>	<i>Arrhythmogenic right ventricular cardiomyopathy/dysplasia</i>
<i>AS</i>	<i>Andersen's syndrome</i>
<i>A_{slow}</i>	<i>Slow amplitude</i>
<i>AVN</i>	<i>atrioventricular node</i>
<i>bp</i>	<i>Base pair</i>
<i>BrS</i>	<i>Brugada syndrome</i>
<i>C</i>	<i>Capacitance</i>
<i>Ca²⁺</i>	<i>Calcium ion</i>
<i>CACNA1C</i>	<i>Ca_v1.2 cardiac L-type calcium channel gene</i>
<i>cAMP</i>	<i>Cyclic adenosine monophosphate</i>
<i>CAV3</i>	<i>Caveolin 3</i>
<i>CHO-K1</i>	<i>Chinese hamster ovary cells (K1 clone)</i>
<i>C_m</i>	<i>Membrane capacitance</i>
<i>C_{pip}</i>	<i>Pipette capacitance</i>
<i>dHPLC</i>	<i>Denaturing high performance liquid chromatography</i>
<i>ECG</i>	<i>Electrocardiogram</i>
<i>EDTA</i>	<i>Ethylene diamine tetra-acetic acid</i>
<i>EGFP</i>	<i>Enhanced green fluorescent protein</i>
<i>EGTA</i>	<i>Ethylene glycol tetraacetic acid</i>
<i>Ex</i>	<i>Exon</i>
<i>F</i>	<i>Farads</i>
<i>FBS</i>	<i>Fetal bovine serum</i>
<i>FDCM</i>	<i>Familial dilated cardiomyopathy</i>
<i>G</i>	<i>Conductance</i>
<i>GFP</i>	<i>Green fluorescent protein</i>
<i>G_{max}</i>	<i>Maximum conductance</i>
<i>GPD1-L</i>	<i>Glycerol-3-phosphate dehydrogenase 1-like</i>
<i>GΩ</i>	<i>Giga Ohms</i>
<i>HCM</i>	<i>Hypertrophic cardiomyopathy</i>
<i>HEK293</i>	<i>Human embryonic kidney cells</i>
<i>HEPES</i>	<i>Hydroxyethyl-piperazineethanesulfonic acid</i>
<i>HERG</i>	<i>Human ether-a-go-go-related gene</i>
<i>hH1</i>	<i>Cardiac sodium channel α-subunit</i>
<i>I</i>	<i>Current</i>
<i>I_{Ca}</i>	<i>L-type calcium current</i>
<i>I_K</i>	<i>Delayed rectifier current</i>
<i>I_{Kr}</i>	<i>Rapid delayed rectifier potassium current</i>
<i>I_{Ks}</i>	<i>Slow delayed rectifier potassium current</i>
<i>I_{Kto}</i>	<i>Transient outward potassium current</i>
<i>I_{max}</i>	<i>Maximum current</i>
<i>I_{Na}</i>	<i>Sodium current</i>

<i>IRES</i>	<i>Internal ribosome entry site</i>
<i>k</i>	<i>Slope factor</i>
K^+	<i>Potassium ion</i>
$K_2\text{-ATP}$	<i>Adenosine triphosphate dipotassium salt</i>
<i>Kb</i>	<i>Kilobases</i>
<i>KCNE1</i>	<i>Potassium voltage-gated channel, Isk-related family, member 1</i>
<i>KCNE2</i>	<i>Potassium voltage-gated channel, Isk-related family, member 2 gene</i>
<i>KCNE3</i>	<i>Potassium voltage-gated channel, Isk-related family, member 3 gene</i>
<i>KCNH2</i>	<i>Rapid delayed potassium channel gene</i>
<i>KCNJ2</i>	<i>Potassium inwardly-rectifying channel, subfamily J, member 2 gene</i>
<i>KCNQ1</i>	<i>Slow delayed potassium channel gene</i>
<i>kDa</i>	<i>Kilodalton</i>
<i>KHz</i>	<i>Kilohertz</i>
$K_v\text{LQT1}$	<i>Potassium voltage-gated channel, KQT-like subfamily, member 1</i>
<i>LQTS</i>	<i>Long QT syndrome</i>
$M\Omega$	<i>Mega Ohms</i>
<i>MinK</i>	<i>Potassium voltage-gated channel subfamily E member</i>
<i>MiRP1</i>	<i>MinK-related peptide 1</i>
<i>mV</i>	<i>Millivolts</i>
Na^+	<i>Sodium ion</i>
$Na_v\ 1.5$	<i>Cardiac sodium channel α-subunit</i>
<i>PAS</i>	<i>Per-Arnt-Sim domain</i>
<i>PCR</i>	<i>Polymerase chain reaction</i>
<i>PIP2</i>	<i>Phosphatidylinositol-4,5-bisphosphate</i>
<i>PKA</i>	<i>Protein Kinase A</i>
<i>R</i>	<i>Resistance</i>
R_a	<i>Access resistance</i>
R_{leak}	<i>Leak resistance</i>
R_m	<i>Membrane resistance</i>
R_{patch}	<i>Patch resistance</i>
R_{pip}	<i>Pipette resistance</i>
<i>S</i>	<i>Siemens</i>
<i>SAN</i>	<i>Sinoatrial node</i>
<i>SCD</i>	<i>Sudden cardiac death</i>
<i>SCN4B</i>	<i>Sodium channel β-subunit Navβ4</i>
<i>SCN5A</i>	<i>Cardiac sodium channel α-subunit</i>
<i>SNTA1</i>	<i>Syntrophin alpha 1</i>
<i>T</i>	<i>Temperature</i>
T_a	<i>Annealing temperature</i>
<i>TD</i>	<i>Touch-down</i>
<i>TS</i>	<i>Timothy syndrome</i>
<i>tsA201</i>	<i>SV40 temperature-sensitive T antigen cells</i>
<i>TTX</i>	<i>Tetrodotoxin</i>
<i>UTR</i>	<i>Untranslated region</i>
<i>V</i>	<i>Voltage</i>
$V_{1/2}$	<i>Membrane potential at half-maximal activation</i>
V_{ion}	<i>Reversal potential of ion</i>
V_m	<i>Membrane potential</i>

V_{rev}	<i>Reversal potential</i>
WT	<i>Wild-type</i>
ΔV	<i>Electrochemical gradient</i>
τ	<i>Time constant</i>
Ω	<i>Ohms</i>

ACKNOWLEDGEMENTS

Firstly, I want to thank my supervisor Prof. Francesco Salvatore to gave me the opportunity to work in his workgroup. I thank also him for his helpfulness and for great advices. I want thank my co-tutor Prof.ssa Giulia Frisso; she constantly guided me with her scientific attitude during my PhD program. She was very patient, helpful and his contribute allowed me to increase my scientific knowledge. Thank you because she trusted me. I would like to thanks Prof. Alfred L. George for the friendly welcome in his laboratory during my USA experience. He helped me to expand my scientific horizons thanks to his huge scientific knowledge.

I have absolutely to thank my lab-friend for funny and crazy moments but also for “high science” discussions.

The last, but not the least, I thank my girlfriend Giusy; she was very close to me also when I was far away.

Thank you very much

REFERENCES

- ✚ Abbott GW, Sesti F, Splawski I, Buck ME, Lehmann MH, Timothy KW, Keating MT, Goldstein SA. MiRP1 forms IKr potassium channels with HERG and is associated with cardiac arrhythmia. *Cell* 1999; 97:175-187;
- ✚ Abriel H, Kass RS. Regulation of the voltage-gated cardiac sodium channel Nav1.5 by interacting proteins. *Trends in Cardiovascular Medicine* 2005; 15:35-40;
- ✚ Amin AS, Asghari-roodsari A, Tan HL. Cardiac sodium channelopathies. *European Journal Of Physiology* 2009; 3:120-135;
- ✚ Amin AS, Tan HL, Wilde AA. Cardiac ion channels in health and disease. *Heart Rhythm* 2010; 7:117-126;
- ✚ Antzelevitch C, Brugada P, Borggrefe M, Brugada J, Brugada R, Corrado D, Gussak I, LeMarec H, Nademanee K, Perez Riera AR, Shimizu W, Schulze-Bahr E, Tan H, Wilde A. Brugada syndrome: report of the second consensus conference: endorsed by the heart rhythm society and the european heart rhythm association. *Circulation* 2005; 111:659-670;
- ✚ Antzelevitch C, Brugada P, Brugada J, Brugada R, Towbin JA, Nademanee K. Brugada syndrome: 1992–2002: a historical perspective. *Journal of American College of Cardiology* 2003; 41:1665-1671;
- ✚ Antzelevitch C, Pollevick GD, Cordeiro JM, Casis O, Sanguinetti MC, Aizawa Y, Guerchicoff A, Pfeiffer R, Oliva A, Wollnik B, Gelber P, Bonaros EP Jr, Burashnikov E, Wu Y, Sargent JD, Schickel S, Oberheiden R, Bhatia A, Hsu LF, Haïssaguerre M, Schimpf R, Borggrefe M, Wolpert C. Loss-of-function mutations in the cardiac calcium channel underlie a new clinical entity characterized by ST-segment elevation, short QT intervals, and sudden cardiac death. *Circulation* 2007; 115:442-449;
- ✚ Antzelevitch C. Electrical heterogeneity, cardiac arrhythmias, and the sodium channel. *Circulation Research* 2000; 87:964-965;
- ✚ Antzelevitch C. Molecular genetics of arrhythmias and cardiovascular conditions associated with arrhythmias. *Journal of Cardiovascular Electrophysiology* 2003; 14:1259-1272;
- ✚ Balsler JR, Nuss HB, Chiamvimonvat N, Pérez-García MT, Marban E, Tomaselli GF. External pore residue mediates slow inactivation in mu 1 rat skeletal muscle sodium channels. *Journal of Physiology* 1996; 494:431-442;
- ✚ Balsler JR. The cardiac sodium channel: gating function and molecular pharmacology. *Journal of Molecular and Cell Cardiology* 2001; 33:599-613;

- ✚ Barhanin J, Lesage F, Guillemare E, Fink M, Lazdunski M, Romey G. K(V)LQT1 and IsK (minK) proteins associate to form the I(Ks) cardiac potassium current. *Nature* 1996; 384: 78-80;
- ✚ Benito B, Brugada J, Brugada R, Brugada P. Brugada syndrome. *Revista Espanola de Cardiologia* 2009; 62:1297-1315;
- ✚ Benito B, Brugada R, Brugada J, Brugada P. Brugada syndrome. *Progress in Cardiovascular Disease* 2008; 51:1-22;
- ✚ Bennett PB, Yazawa K, Makita N, George AL Jr. Molecular mechanism for an inherited cardiac arrhythmia. *Nature* 1995; 376:683-685;
- ✚ Bezzina CR, Rook MB, Wilde AA. Cardiac sodium channel and inherited arrhythmia syndromes. *Cardiovascular Research* 2001; 47:257-271;
- ✚ Brink PA, Crotti L, Corfield V, Goosen A, Durrheim G, Hedley P, Heradien M, Geldenhuys G, Vanoli E, Bacchini S, Spazzolini C, Lundquist AL, Roden DM, George AL Jr, Schwartz PJ. Phenotypic variability and unusual clinical severity of congenital long-QT syndrome in a founder population. *Circulation* 2005; 112:2602-2610.
- ✚ Canùn S, Perez N, Beirana LG. Andersen syndrome autosomal dominant in three generations. *American Journal of Medical Genetics* 1999; 85:147-156.
- ✚ Cayabyab FS, Schlichter LC. Regulation of an ERG K⁺ current by Src tyrosine kinase. *Journal of Biological Chemistry* 2002; 277:13673-13681;
- ✚ Chen J, Zou A, Splawski I, Keating MT, Sanguinetti MC. Long QT syndrome-associated mutations in the Per-Arnt-Sim (PAS) domain of HERG potassium channels accelerate channel deactivation. *Journal of Biological Chemistry* 1999; 274:10113-10118;
- ✚ Cormier JW, Rivolta I, Tateyama M, Yang AS, Kass RS. Secondary structure of the human cardiac Na⁺ channel C terminus: evidence for a role of helical structures in modulation of channel inactivation. *Journal of Biological Chemistry* 2002; 277:9233-9241;
- ✚ Crawley JN. *Current protocols in neuroscience*. New York (USA), Wiley & Sons (1997): 100-120;
- ✚ Delpón E, Cordeiro JM, Núñez L, Thomsen PE, Guerchicoff A, Pollevick GD, Wu Y, Kanters JK, Larsen CT, Hofman-Bang J, Burashnikov E, Christiansen M, Antzelevitch C. Functional effects of KCNE3 mutation and its role in the development of Brugada syndrome. *Circulation, Arrhythmia and Electrophysiology* 2008; 1:209-218;
- ✚ Dennis A, Wang L, Wan X, Ficker E. HERG channel trafficking: novel targets in drug-induced long QT syndrome. *Biochemical Society Transaction* 2007; 35:1060-1063;

- ✚ Di Diego JM, Cordeiro JM, Goodrow RJ, Fish JM, Zygmunt AC, Pérez GJ, Scornik FS, Antzelevitch C. Ionic and cellular basis for the predominance of the Brugada syndrome phenotype in males. *Circulation* 2002; 106:2004-2011
- ✚ Doyle DA, Morais Cabral J, Pfuetzner RA, Kuo A, Gulbis JM, Cohen SL, Chait BT, MacKinnon R. The structure of the potassium channel: molecular basis of K⁺ conduction and selectivity. *Science* 1998; 280:69-77;
- ✚ Fozzard HA, Haber E. Rhythmic excitation of the heart. In *The heart and cardiovascular system: scientific foundation*. New York (USA): Raven Press (1991):3-10;
- ✚ Franqueza L, Lin M, Shen J, Splawski I, Keating MT, Sanguinetti MC. Long QT syndrome-associated mutations in the S4-S5 linker of KvLQT1 potassium channels modify gating and interaction with minK subunits. *Journal of Biological Chemistry* 1999; 274:21063-21070;
- ✚ Gellens ME, George AL Jr, Chen LQ, Chahine M, Horn R, Barchi RL, Kallen RG. Primary structure and functional expression of the human cardiac tetrodotoxin-insensitive voltage-dependent sodium channel. *Proceeding of the National Academy of Science of USA* 1992; 89:554-558;
- ✚ George AL Jr, Varkony TA, Drabkin HA, Han J, Knops JF, Finley WH, Brown GB, Ward DC, Haas M. Assignment of the 1 human heart tetrodotoxin-resistant voltage-gated Na channel α -subunit gene (SCN5A) to band 3p21. *Cytogenetics and Cell Genetics* 1995; 68:67-70;
- ✚ George AL. Genetic modulation of impaired cardiac conduction sodium channel β 4 subunit missing in action. *Circulation Research* 2009; 104:1238-1239;
- ✚ George AL. Inherited disorders of voltage-gated sodium channels. *The Journal of Clinical Investigation* 2005; 115:1991-1999;
- ✚ Goldenberg I, Moss AJ. Long QT syndrome. *Journal of the American College of Cardiology* 2008; 51:2291-2300
- ✚ Grant AO. Cardiac ion channels. *Circulation. Arrhythmia and electrophysiology* 2009; 2:185-194;
- ✚ Hedley PL, Jorgensen P Schlamowitz S, Wangari R, Moolman-Smook J, Brink PA, Kanters JK, Corfield VA, Christiansen M. The genetic basis of long QT and short QT syndromes: a mutation update. *Human Mutation* 2009; 30:1486-1511;
- ✚ Heinemann SH. Guide to data acquisition and analysis. In *Single-Channel Recording*. New York (USA), Plenum (1995):53-96;

- ✚ Hermida JS, Lemoine JL, Aoun FB, Jarry G, Rey JL, Quiret JC. Prevalence of the Brugada syndrome in an apparently healthy population. *American Journal of Cardiology* 2000; 86:91-94;
- ✚ Hille B. Selective permeability: independence. In *Ion channels of excitable membranes*. Sunderland (UK), Sinauer Association Inc. (2001):249-271;
- ✚ Honoré E, Attali B, Romey G, Heurteaux C, Ricard P, Lesage F, Lazdunski M, Barhanin J. Cloning, expression, pharmacology and regulation of a delayed rectifier K⁺ channel in mouse heart. *EMBO Journal* 1991; 10:2805-2811;
- ✚ <http://www.fsm.it/cardmoc/>;
- ✚ <http://www.ncbi.nlm.nih.gov/> ; MIM #192500;
- ✚ Jervell A and Lange-Nielsen F. Congenital deaf-mutism, functional heart disease with prolongation of the QT interval and sudden death. *American Heart Journal* 1957; 54: 59-68;
- ✚ Jones EM, Roti Roti EC, Wang J, Delfosse SA, Robertson GA. Cardiac IKr channels minimally comprise hERG 1a and 1b subunits. *Journal of Biological Chemistry* 2004 ;279:44690-44694;
- ✚ Keating MT, Sanguinetti MC. Molecular and cellular mechanisms of cardiac arrhythmias. *Cell* 2001; 104:569-580;
- ✚ Kies P, Wichter T, Schäfers M, Paul M, Schäfers KP, Eckardt L, Stegger L, Schulze-Bahr E, Rimoldi O, Breithardt G, Schober O, Camici PG. Abnormal myocardial presynaptic norepinephrine recycling in patients with Brugada syndrome. *Circulation* 2004; 110:3017-3022;
- ✚ Kornreich BG. The patch clamp technique: Principles and technical considerations. *Journal of Veterinary Cardiology* 2007; 9:25-37;
- ✚ Kurokawa J, Motoike HK, Rao J, Kass RS. Regulatory actions of the A-kinase anchoring protein Yotiao on a heart potassium channel downstream of PKA phosphorylation. *Proceeding of National Academy of Sciences of USA* 2004;101: 16374-16378;
- ✚ Langer GA. Ion channel in cardiac muscle. In *The myocardium*. San Diego (USA), Academic Press (1997):81-132;
- ✚ Lee MP, Hu RJ, Johnson LA, Feinberg AP. Human KVLQT1 gene shows tissue-specific imprinting and encompasses Beckwith-Wiedemann syndrome chromosomal rearrangements. *Nature Genetics* 1997; 15:181-185;
- ✚ Lees-Miller JP, Kondo C, Wang L, Duff HJ. Electrophysiological characterization of an alternatively processed ERG K⁺ channel in mouse and human hearts. *Circulation Research* 1997; 81:719-726;
- ✚ London B, Michalec M, Mehdi H, Zhu X, Kerchner L, Sanyal S, Viswanathan PC, Pfahnl AE, Shang LL, Madhusudanan M, Baty

- CJ, Lagana S, Aleong R, Gutmann R, Ackerman MJ, McNamara DM, Weiss R, Dudley SC Jr.. Mutation in glycerol-3-phosphate dehydrogenase 1 like gene (GPD1-L) decreases cardiac Na⁺ current and causes inherited arrhythmias. *Circulation* 2007; 116:2260-2268;
- ✚ Matsuo K, Akahoshi M, Seto S, Yano K. Disappearance of the Brugada-type electrocardiogram after surgical castration: a role for testosterone and an explanation for the male preponderance. *Pacing and Clinical Electrophysiology* 2003; 26:1551-1553;
 - ✚ McPhee JC, Ragsdale DS, Scheuer T, Catterall WA. A critical role for transmembrane segment IVS6 of the sodium channel α subunit in fast inactivation. *Journal of Biological Chemistry* 1995; 270:12025-12034;
 - ✚ Meadows LS, Isom LL. Sodium channels as macromolecular complexes: implications for inherited arrhythmia syndromes. *Cardiovascular Research* 2005; 67:448-58;
 - ✚ Miyasaka Y, Tsuji H, Yamada K, Tokunaga S, Saito D, Imuro Y, Matsumoto N, Iwasaka T. Prevalence and mortality of the Brugada-type electrocardiogram in one city in Japan. *Journal of American College of Cardiology* 2001; 38:771-774;
 - ✚ Miyazaki T, Mitamura H, Miyoshi S, Soejima K, Aizawa Y, Ogawa S. Autonomic and antiarrhythmic drug modulation of ST segment elevation in patients with Brugada syndrome. *Journal of American College of Cardiology* 1996; 27:1061-1070;
 - ✚ Mohler PJ, Schott JJ, Gramolini AO, Dilly KW, Guatimosim S, duBell WH, Song LS, Haurogné K, Kyndt F, Ali ME, Rogers TB, Lederer WJ, Escande D, Le Marec H, Bennett V. Ankyrin-B mutation causes type 4 long-QT Cardiac arrhythmia and sudden cardiac death. *Nature* 2003;421:634-639;
 - ✚ Molleman A. Basic Theoretical principles. In *Patch clamping*. Chichester (UK), Wiley & Sons (2002):30-38;
 - ✚ Morais Cabral JH, Lee A, Cohen SL, Chait BT, Li M, Mackinnon R. Crystal structure and functional analysis of the HERG potassium channel N terminus: a eukaryotic PAS domain. *Cell* 1998; 95:649-655
 - ✚ Morita H, Wu J, Zipes DP. The QT syndromes: long and short. *Lancet* 2008; 372:750-763;
 - ✚ Napolitano C, Priori SG, Schwartz PJ, Bloise R, Ronchetti E, Nastoli J, Bottelli G, Cerrone M, Leonardi S. Genetic testing in the long QT syndrome: development and validation of an efficient approach to genotyping in clinical practice. *The Journal of the American Medical Association* 2005; 294:3027-3028;

- ✚ Neher E. Unit conductance studies in biological membranes. In: *Techniques in Cellular Physiology*. Amsterdam (NE), Elsevier (1981):41-55;
- ✚ Neyroud N, Richard P, Vignier N, Donger C, Denjoy I, Demay L, Shkolnikova M, Pesce R, Chevalier P, Hainque B, Coumel P, Schwartz K, Guicheney P. Genomic organization of the KCNQ1 K⁺ channel gene and identification of C-terminal mutations in the long QT syndrome. *Circulation Research* 1999; 84:290-297;
- ✚ Noble D, Tsien RW. Outward membrane currents activated in the plateau range of potentials in cardiac Purkinje fibres. *Journal of Physiology* 1969; 200:205–31;
- ✚ Ogden D, Stanfield P. Patch clamp techniques for single channel and whole-cell recording. In *Microelectrode techniques*. Cambridge (UK), Company of Biologists (1994):53-78;
- ✚ Park KH, Piron J, Dahimene S, Mérot J, Baró I, Escande D, Lousouarn G. Impaired KCNQ1-KCNE1 and phosphatidylinositol-4,5-bisphosphate interaction underlies the long QT syndrome. *Circulation Research* 2005; 96: 730-739;
- ✚ Paulussen A, Raes A, Matthijs G, Snyders DJ, Cohen N, Aerssens J. A novel mutation (T65P) in the PAS domain of the human potassium channel HERG results in the long QT syndrome by trafficking deficiency. *Journal of Biological Chemistry* 2002; 277:48610–48616;
- ✚ Pérez-García MT, Chiamvimonvat N, Ranjan R, Balsler JR, Tomaselli GF, Marban E. Mechanisms of sodium/calcium selectivity in sodium channels probed by cysteine mutagenesis and sulfhydryl modification. *Biophysical Journal* 1997; 72:989-996;
- ✚ Phartiyal P, Sale H, Jones EM, Robertson GA. Endoplasmic reticulum retention and rescue by heteromeric assembly regulate human ERG 1a/1b surface channel composition. *Journal of Biological Chemistry* 2008; 283:3702-3707;
- ✚ Plaster NM, Tawil R, Tristani-Firouzi M, Canún S, Bendahhou S, Tsunoda A, Donaldson MR, Iannaccone ST, Brunt E, Barohn R, Clark J, Deymeer F, George AL Jr, Fish FA, Hahn A, Nitu A, Ozdemir C, Serdaroglu P, Subramony SH, Wolfe G, Fu YH, Ptáček LJ.. Mutations in Kir2.1 cause the developmental and episodic electrical phenotypes of Andersen's syndrome. *Cell* 2001; 105:511-519;
- ✚ Potet F, Scott JD, Mohammad-Panah R, Escande D, Baró I. AKAP proteins anchor cAMP- dependent protein kinase to KvLQT1/IsK channel complex. *American Journal of Physiology. Heart and Circulation Physiology* 2001; 280: H2038-H2045;

- ✚ Priori SG, Napolitano C, Vincentini A. Inherited arrhythmia syndromes: applying the molecular biology and genetics to the clinical management. *Journal of Interventional Cardiac Electrophysiology* 2003; 9:93-101;
- ✚ Priori SG, Napolitano C, Gasparini M, Pappone C, Della Bella P, Giordano U, Bloise R, Giustetto C, De Nardis R, Grillo M, Ronchetti E, Faggiano G, Nastoli J. Natural history of Brugada syndrome: insights for risk stratification and management. *Circulation* 2002; 105:1342-1347;
- ✚ Priori SG. Inherited arrhythmogenic diseases: the complexity beyond monogenic disorders. *Circulation Research* 2004; 94:140-145;
- ✚ Pusch M. Increase of the single-channel conductance of KvLQT1 potassium channels induced by the association with minK. *Pflügers Archiv* 1998; 437:172-175;
- ✚ Roden DM, Balser JR, George AL Jr, Anderson ME. Cardiac ion channels. *Annual review of physiology* 2002; 64:431-475;
- ✚ Sakmann B, Neher E. Geometric parameters of pipettes and membrane patches. In *Single-Channel Recording*. New York (USA), Plenum (1995):637-650;
- ✚ Sanguinetti MC, Jurkiewicz NK. Two components of cardiac delayed rectifier K⁺ current. Differential sensitivity to block by class III antiarrhythmic agents. *Journal of General Physiology* 1990; 96:195-215;
- ✚ Sanguinetti MC, Curran ME, Zou A, Shen J, Spector PS, Atkinson DL, Keating MT. Coassembly of K(V)LQT1 and minK (IsK) proteins to form cardiac I(Ks) potassium channel. *Nature* 1996; 384:80-83;
- ✚ Sanguinetti MC, Jiang C, Curran ME, Keating MT. A mechanistic link between an inherited and an acquired cardiac arrhythmia: HERG encodes the IKr potassium channel. *Cell* 1995; 81:299-307;
- ✚ Satin J, Kyle JW, Chen M, Rogart RB, Fozzard HA. The cloned cardiac Na channel α -subunit expressed in *Xenopus* oocytes show gating and blocking properties of native channels. *Journal of Membrane Biology* 1992; 130:11-22;
- ✚ Schulze-Bahr E, Wang Q, Wedekind H, Haverkamp W, Chen Q, Sun Y, Rubie C, Hördt M, Towbin JA, Borggrefe M, Assmann G, Qu X, Somberg JC, Breithardt G, Oberti C, Funke H.. KCNE1 mutations cause Jervell and Lange-Nielsen syndrome. *Nature genetics* 1997; 17:267-268;
- ✚ Schwartz JR, Bauer CK. Function of erg K⁺ channels in excitable cells. *Journal of Cellular and Molecular Medicine* 2004; 8:22-30;
- ✚ Schwartz PJ, Moss AJ, Vincent GM, Crampton RS. Diagnostic criteria for long QT syndrome. An update. *Circulation* 1993; 88:782-784;

- ✚ Schwartz PJ, Priori SG, Spazzolini C, Moss AJ, Vincent GM, Napolitano C, Denjoy I, Guicheney P, Breithardt G, Keating MT, Towbin JA, Beggs AH, Brink P, Wilde AA, Toivonen L, Zareba W, Robinson JL, Timothy KW, Corfield V, Wattanasirichaigoon D, Corbett C, Haverkamp W, Schulze-Bahr E, Lehmann MH, Schwartz K, Coumel P, Bloise R. Genotype-phenotype correlation in the long-QT syndrome gene-specific triggers for life-threatening arrhythmias. *Circulation* 2001; 103:89-95;
- ✚ Splawski I, Timothy KW, Decher N, Kumar P, Sachse FB, Beggs AH, Sanguinetti MC, Keating MT. Severe Arrhythmias Disorders Caused By Cardiac L-Type Calcium Channel Mutations. *Proceedings of the National Academy of Science in the USA* 2005; 102:8089-8096;
- ✚ Stühmer W, Conti F, Suzuki H, Wang XD, Noda M, Yahagi N, Kubo H, Numa S. Structural parts involved inactivation and inactivation of the sodium channel. *Nature* 1989; 339:597-603;
- ✚ Takumi T, Ohkubo H, Nakanishi S. Cloning of a membrane protein that induces a slow voltage-gated potassium current. *Science* 1988; 242:1042–1045;
- ✚ Tan HL. Sodium channel variants in heart disease: expanding horizons. *Journal of Cardiovascular Electrophysiology* 2006; 17:S151– S157;
- ✚ Tristani-Firouzi M, Jensen JL, Donaldson MR, Sansone V, Meola G, Hahn A, Bendahhou S, Kwiecinski H, Fidzianska A, Plaster N, Fu YH, Ptacek LJ, Tawil R. Functional and clinical characterization of KCNJ2 mutations associated with LQT7 (Andersen Syndrome). *Journal of Clinical Investigation* 2002; 110:381–388;
- ✚ Vatta M, Ackerman MJ, Ye B, Makielski JC, Ughanze EE, Taylor EW, Tester DJ, Balijepalli RC, Foell JD, Li Z, Kamp TJ, Towbin JA. Mutant caveolin-3 induces persistent late sodium current and is associated with long-QT syndrome. *Circulation* 2006; 114:2104-2112;
- ✚ Vatta M, Dumaine R, Antzelevitch C, Brugada R, Li H, Bowles NE, Nademanee K, Brugada J, Brugada P, Towbin JA. Novel mutations in domain I of SCN5A cause Brugada syndrome. *Molecular Genetics and Metabolism* 2002; 75:317-324;
- ✚ Vohra J. The long QT syndrome. *Heart, Lung and Circulation* 2007; 16:S5-S12;
- ✚ Wang DW, Yazawa K, George AL Jr, Bennett PB. Characterization of human cardiac Na⁺ channel mutations in the congenital long QT syndrome. *Proceeding of National Academy of Sciences of USA* 1996; 93:13200-13205;

- ✚ Wang J, Trudeau MC. The mechanism of N-terminal regulation of deactivation in HERG potassium channels. *Biophysics Journal* 1998; 74:A254;
- ✚ Wang Q, Curran ME, Splawski I, Burn TC, Millholland JM, VanRaay TJ, Shen J, Timothy KW, Vincent GM, de Jager T, Schwartz PJ, Toubin JA, Moss AJ, Atkinson DL, Landes GM, Connors TD, Keating MT. Positional cloning of a novel potassium channel gene—KVLQT1 mutations cause cardiac arrhythmias. *Nature Genetics* 1996; 12:17-23;
- ✚ West JW, Patton DE, Scheuer T, Wang Y, Goldin AL, Catterall WA. A cluster of hydrophobic amino acid residues required for fast Na(+)-channel inactivation. *Proceeding of National Academy of Sciences of USA* 1992; 89:10910-10914;
- ✚ Westermann M, Steiniger F, Richter W. Belt-like localisation of caveolin in deep caveolae and its re-distribution after cholesterol depletion. *Histochemistry and Cell Biology* 2005; 123:613-620;
- ✚ Wilde AA, Antzelevitch C, Borggrefe M, Brugada J, Brugada R, Brugada P, Corrado D, Hauer RN, Kass RS, Nademanee K, Priori SG, Towbin JA. Proposed diagnostic criteria for the Brugada syndrome: Consensus Report. *Circulation* 2002; 106:2514-2519;
- ✚ Wilde AA, Antzelevitch C, Borggrefe M, Brugada J, Brugada R, Brugada P, Corrado D, Hauer RN, Kass RS, Nademanee K, Priori SG, Towbin JA. Proposed diagnostic criteria for the Brugada syndrome. *European Heart Journal* 2002; 23:1648-1654;
- ✚ Wolf CM and Berul CI. Molecular mechanisms of inherited arrhythmia. *Current Genomics* 2008; 9:160-168;
- ✚ Yan GX, Antzelevitch C. Cellular basis for the Brugada syndrome and other mechanisms of arrhythmogenesis associated with ST-segment elevation. *Circulation* 1999; 100:1660-1666;
- ✚ Yang P, Kanki H, Drolet B, Yang T, Wei J, Viswanathan PC, Hohnloser SH, Shimizu W, Schwartz PJ, Stanton M, Murray KT, Norris K, George AL Jr, Roden DM. Allelic variants in long-QT disease genes in patients with drug-associated torsades de pointes. *Circulation* 2002; 105:1943-1948;
- ✚ Yellen G, Jurman ME, Abramson T, MacKinnon R. Mutations affecting internal TEA blockade identify the pore-forming region of a K channel. *Science* 1991; 251:939-942.